~~Oblique basin inversion leads to f~~Fold localisation at ~~bounding pre-existing normal~~ faults: Field observations and a~~A~~nalogue modelling of the Achental structure, Northern Calcareous Alps, Austria

Willemijn Sarah Maria Theresia van Kooten[1,2], Hugo Ortner[1], Ernst Willingshofer[3], Dimitrios Sokoutis[3,4], Alfred Gruber[5], Thomas Sausgruber[6]

[1]Institut für Geologie, Universität Innsbruck, Innsbruck, 6020, Austria
[2]Department of Digital Business & Software Engineering, MCI - The Entrepreneurial School, Innsbruck, 6020, Austria
[3]Department of Earth Sciences, Utrecht University, Utrecht, 3584 CB, Netherlands
[4]Department of Geosciences, University of Oslo, Oslo, Norway
[5]Geologische Bundesanstalt für Österreich (GBA), Wien, 1030, Austria
[6]die.wildbach, Wilhelm-Greil-Straße 9 6020 Innsbruck, Austria

Correspondence to: Willemijn S.M.T. van Kooten (willemijn.vankooten@mci.edu), ORCID: 0000-0002-9784-444X

Abstract

Within the Northern Calcareous Alps fold-and-thrust belt of the Eastern Alps, multiple pre-shortening deformation phases have contributed to the structural grain that controlled localisation~~sed~~ of deformation at later stages. In particular, Jurassic rifting and opening of the Alpine Tethys led to the formation of extensional basins at the northern margin of the Apulian plate. Subsequent Cretaceous shortening within the Northern Calcareous Alps produced the enigmatic Achental structure, which forms a sigmoidal transition zone between two E-W striking major synclines. One of the major complexities of the Achental structure is that all structural elements are oblique to the Cretaceous direction of shortening. Its sigmoidal form was, therefore, proposed to be a result of forced folding at the boundaries of the Jurassic Achental basin. This study analyses the structural evolution of the Achental structure through integrating field observations with crustal-scale physical analogue modellings, to elucidate the influence of pre-existing crustal heterogeneities on oblique basin inversion ~~and the prerequisites for the formation of a sigmoidal hanging wall that outlines former basin margins~~. From brittle-ductile models, we infer that oblique shortening ~~oblique to~~ of pre-existing extensional faults can lead to the localisation of ~~thrust faults~~deformation at the pre-existing structure ~~within~~ and predicts thrust and fold structures that are consistent with field observations~~a single deformation phase~~. Prerequisites are ~~1)~~ a weak basal décollement that is offset by an existing normal fault and~~, 2)~~ the presence of topography in the hinterland during~~, 3) a~~ thin-skinned deformation ~~style~~. Consequently, the Achental low-angle thrust and ~~corresponding~~sigmoidal fold trains~~s~~ was able to localise ~~exactly~~ at the former Jurassic basin margin, with a vergence opposite to the ~~Jurassic~~ controlling normal fault, creating the characteristic sigmoidal morphology during a single phase of NW-directed shortening.

1 Introduction

The deformational style and tectonic history of Earth's orogenic belts is strongly influenced by pre-existing structural elements. In particular, structures formed by shortening and inversion of pre-orogenic basins are often governed by the reactivation of former basin-bounding normal faults as summarised by Turner and Williams (2004) or Cooper and Warren (2020). Consequently, previous studies have focused on the mechanics of fault reactivation (e.g., Etheridge, 1986; Nielsen & Hansen, 2000; Sibson, 1995; Tong & Yin, 2011), or present regional case studies of basin inversion (e.g., Héja et al., 2022; Kley et al., 2005; Thorwart et al., 2021). Existing literature presenting analogue and numerical modelling of inversional settings is extensive and includes the re-activation

of planar and listric extensional fault systems of various orientation as well as basin inversion orthogonal or oblique to the basin axes (e.g., Amilibia et al., 2005; Bonini, 1998; Brun & Nalpas, 1996; Buchanan & McClay, 1992; S. J. H. Buiter & Pfiffner, 2003; Dubois et al., 2002; Konstantinovskaya et al., 2007; Koopman et al., 1987; Sassi et al., 1993; Zwaan et al., 2022). In most models, newly formed reverse faults are synthetic to the pre-existing normal faults (see also Bonini et al., 2012; their Figure 3), whereas the formation of thrust faults antithetic to the former basin-bounding faults is seldomly described.

In this study, we use an example from the Northern Calcareous Alps (NCA) in Austria (Figure 1~~a~~), in which basin inversion during Alpine orogeny has created a low-angle thrust antithetic to a normal fault bounding a Jurassic extensional basin. In the hanging wall of this thrust, a fold train outlines the margins of this ~~former~~ basin, forming a characteristic sigmoidal shape that has been the subject of geological investigations since the beginning of the 20th century (Ampferer, 1902, 1941; Fuchs, 1944; Nagel, 1975; Nagel et al., 1976; Quenstedt, 1933). We use the example of the Achental structure and its underlying basin geometry as a starting point for analogue modelling, to simulate the oblique inversion of a former extensional basin and the deformation of a brittle-ductile sedimentary succession at its margins. The main aim of this study is to better understand strain localization and associated deformation by folding and thrusting at oblique basin bounding faults. In particular, this study examines whether a sigmoidal hanging wall shape outlining former basin margins can be explained by a single phase of oblique shortening and if so what are the critical rheological and kinematic parameters to obtain such structures. Our modelling results are then compared to the Achental structure, to better understand the formation of complex inversion structures in fold-and-thrust belts.

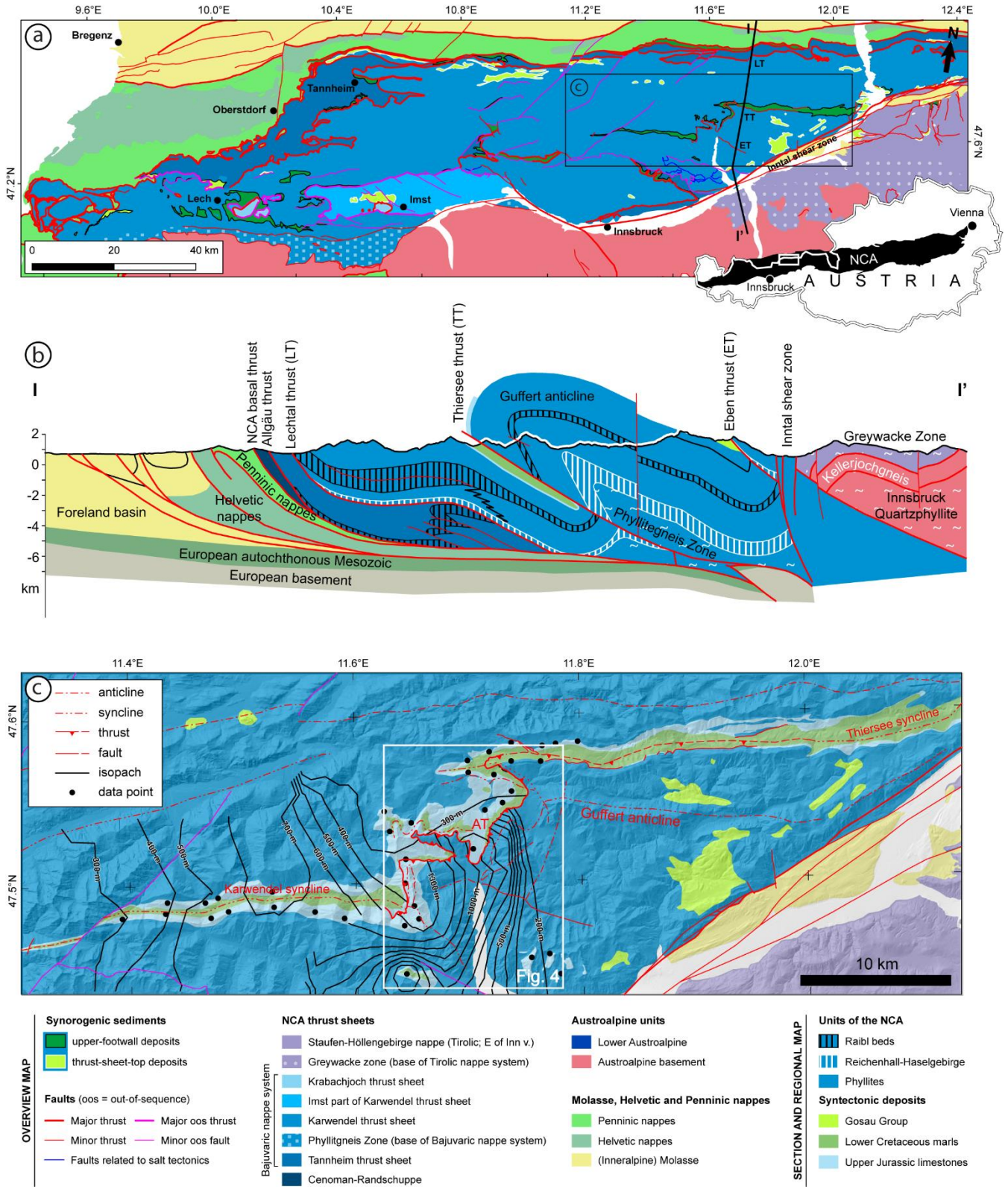

Figure 1: (a) Geological ~~overview~~ map of the Achental structure within the Karwendel thrust sheet. Top inset shows the location of the NCA in Austria. Rectangle shows location of Figure 1c. Modified after Ortner and Kilian (2022). (b) N-S cross-section of the NCA at ~ 11.7°E, crossing the Achental structure. (c) Isopach map of the Upper Jurassic Oberalm Fm, with d~~. The Achental thrust (red line) is given for reference of location. D~~ata compiled from Nagel et al. (1976) and K.-I. Schütz (1979). The h~~H~~anging wall and footwall of the Achental thrust (AT) were contoured separately, single outliers in the data were ignored. Major thickness changes occur from W to E, a maximum is observed in the southern hanging wall of the thrust.

2 Geological setting

The Northern Calcareous Alps (NCA) of Austria have a polyphase tectonic and sedimentary history that started in the Permian. The following evolutionary stages are distinguished (Figure 2):

1) Deposition of a Permian-Triassic carbonate platform succession on the south(east)ern passive margin of Pangaea bordering the Neotethys from the Permian to the end of the Triassic (e.g., Haas et al., 1995; Lein, 1987; Schmid et al., 2004; Schmid et al., 2008; Stampfli et al., 1998). ~~The major part of the Permian-Triassic is carbonate platforms.~~
2) Early to Middle Jurassic rifting and subsequent opening of the Alpine Tethys that separated the Apulian/Adriatic microplate from the European continent lead to subsidence and drowning of the Triassic carbonate platforms (e.g., Faupl & Wagreich, 1999; Froitzheim & Manatschal, 1996; Schmid et al., 2004). R~~ift related subsidence caused the drowning of former Triassic carbonate platforms, r~~ift-related faulting established the normal faults that were inverted during Cretaceous orogeny (Eberli et al., 1993; Ortner et al., 2008).
3) Shortening related to Late Jurassic obduction of Neotethys oceanic crust onto the southeastern Apulian margin heralded inversion of this margin that culminated in the Cretaceous orogeny (Schmid et al., 2004; Stüwe & Schuster, 2010). During the Cretaceous orogeny the NCA were a typical thin-skinned fold-and-thrust belt at the external margin of the Austroalpine orogenic wedge in lower plate position (Eisbacher & Brandner, 1996; Ortner & Kilian, 2022).
4) During the Late Cretaceous this wedge was transported toward the northwestern passive margin of the Apulian plate, which ~~. In the late Cretaceous, this margin~~ became an active margin through subduction of~~where~~ the Alpine Tethys ~~was subducted~~ (Ortner & Sieberer, 2022; Stüwe & Schuster, 2010; Willingshofer et al., 1999).
5) Late Eocene closure of the Alpine Tethys caused collision between the lower, European and upper, Apulian plates and thus a second, Paleogene phase of mountain building, referred to as "Alpine orogeny" (Eisbacher & Brandner, 1996; Ortner, 2003b; Schmid et al., 2004; Stüwe & Schuster, 2010). In the course of this process the Austroalpine units and the NCA fold-and-thrust belt were transported piggyback onto the European margin. Contrasting with Cretaceous orogeny, the Austroalpine wedge formed the upper plate during Paleogene orogeny.

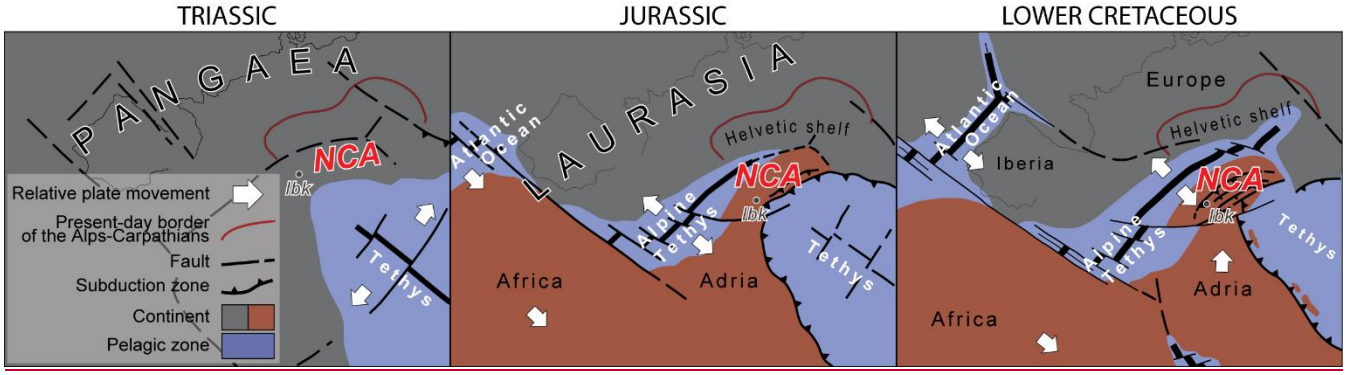

Figure 2: Developmental stages in the tectonic evolution of the Northern Calcareous Alps, modified after Schuster et al. (2019). (a) Permotriassic stage with sedimentation on the passive margin of Pangaea. (b) Early-Middle Jurassic opening of the Alpine Tethys, with sedimentation in basins and on swells. (c) Cretaceous orogeny. (d) Late Cretaceous subduction leading to Late Eocene closure of the Alpine Tethys and Alpine orogeny. The present-day location of Innsbruck (Ibk) is marked.

Relevant for~~The important stages in the frame of~~ this study are the Jurassic rifting that created sedimentary basins~~,~~ and the Cretaceous and Paleogene shortening that led to basin inversion. Jurassic extensional basins formed along intersecting fault systems with N-S trending normal faults and E-W trending transform faults, as ~~studied~~ documented in the Eastern Alps of Switzerland (Eberli, 1985, 1987; Weissert & Bernoulli, 1985). Similar orientations of extensional normal faults have been found in the Western

Alps (Lemoine et al., 1986). The existence ~~In the present day Achensee region, Jurassic extension and the formation~~ of an extensional basin in the Achensee region is indicated by filled fissures that occur in Oberrhätkalk (Gruber et al., 2022), strong lateral thickness variations of (Upper) Jurassic strata (Figure 1b) (Nagel et al., 1976; K.-I. Schütz, 1979) and characteristic breccias that are locally intercalated in basinal Jurassic sediments (Brandner et al., 2011; Channell et al., 1990; Channell et al., 1992; Spieler & Brandner, 1989).

Cretaceous to Paleogene shortening within the NCA is characterized by two separate directions of transport. ~~Whereas d~~During Cretaceous orogeny the thrust sheets of the NCA were transported and stacked in WNW- to NW-direction (Eisbacher & Brandner, 1996), whereas~~during~~ Paleogene ~~orogeny~~ shortening of the NCA fold-and-thrust belt was associated with~~transported in~~ N- to NNE transport~~-~~ directions (Schmid et al., 1996). These differences are well documented within t~~T~~he basement units of the Austroalpine wedge ~~show a clear separation between the Cretaceous and Paleogene stages~~ (Froitzheim et al., 1994), although~~but~~ synorogenic growth strata show continuous shortening within the NCA (Ortner, 2001, 2003a; Ortner et al., 2016; Ortner & Gaupp, 2007).

2.1 Sedimentary succession

The sedimentary succession of the NCA encompasses a late Permian to ~~Early Cretaceous~~Oligocene stratigraph~~yic column~~. The Permotriassic succession reflects subsidence of the south(east)ern passive margin of Pangaea from continental to shallow marine conditions. ~~that reflects the growth of two major Middle and Upper Triassic carbonate platforms and their subsequent drowning (Figure 2).~~ During the Permian-Middle Triassic, the marine ingression of the Tethys led to the formation of a subtidal-supratidal marine environment, where evaporitic Haselgebirge-Reichenhall succession accumulated. The Haselgebirge contains large amounts of halite, gypsum and anhydrite in a shale matrix ~~During the Permian-Middle Triassic, the marine ingression of the Tethys led to the formation of a subtidal-supratidal marine environment, where evaporitic deposits (Haselgebirge) accumulated. The large amounts of halite, gypsum and anhydrite contained within these strata~~ (Leitner & Neubauer, 2011) ~~are the cause of their highly incompetent behavior~~. The thickness of Haselgebirge is highly variable, due to salt ~~diapirism and~~ tectonics and solution, ~~although~~ but a primary thickness of 500-1000 m can be expected (Spötl, 1989: Fig. 2). Lower Triassic sandstones (Alpine Buntsandstein) overlie the Haselgebirge and are followed by ~~the~~ an Anisian limestone-dolostone-evaporite succession (Reichenhall Formation (Fm~~);~~ ~~(~~Figure 3~~2~~). ~~The latter consists of alternating layered dolomite, cellular dolomite and bituminous limestone~~ with a thickness of 80-200 m in the Achensee region (Nagel et al., 1976). The Haselgebirge-Reichenhall succession ~~composes~~ represents a rheologically incompetent part of the stratigraphic column, forming the principal décollement of the NCA (Eisbacher & Brandner, 1995). The Eben thrust (Figure 1) brings the Haselgebirge-Reichenhall succession to the surface in the Achensee region. ~~Furthermore, i~~Its presence in the subsurface has been inferred from depth-extrapolated cross sections based on TRANSALP and industry reflection seismic lines (Auer & Eisbacher, 2003: their Figure 15).

The evaporitic Haselgebirge-Reichenhall succession transitions into a succession of Anisian-Ladinian limestones (Alpine Muschelkalk Group; Bechstädt & Mostler, 1974). These vary from shallow-water, strongly bioturbated mud- to wackestones (e.g., Virgloria Fm, Steinalm Fm) to basin marginal and basinal limestones (Reifling Fm; Rüffer & Zühlke, 1995). The uppermost Alpine Muschelkalk Group interfingers with the Wetterstein limestone (Anisian–Carnian), which forms the first of two major carbonate platforms of the NCA (Figure 3). ~~Lithotypes consist of lagoonal, reefal and forereefal lime- and dolostones with a fossiliferous content of e.g., stromatolithes, oolites, calcareous algae and sponges; and their fragments.~~ Although the Alpine Muschelkalk Group and Wetterstein limestone show a general thickness between 1000 to >2200 m in the Achensee region (Gruber et al., 2022; Nagel et al., 1976; Sausgruber, 1994b), cross sections in Gruber et al. (2022) show a thickness up to 3500 m. These thickness variations

are attributedmight be a result of to salt tectonics in the Triassic (see e.g., Granado et al., 2019; Kilian et al., 2021; Ortner & Kilian, 2022) , however, minibasin margins with typical stratal geometries such as wedges or hooks (Giles & Rowan, 2012) or flaps (Rowan et al., 2016) have not been documented in the Achensee region so far. The Carnian Raibl event marks the abrupt termination of carbonate sedimentation on the Wetterstein platform (). About 400 m of Carnian sandstones, shales, dolomites, evaporites and limestones (Raibl beds) As a result, the Raibl beds (Carnian) overlie the Wetterstein platform unconformably. They consist of sandstones, shales, dolomites, cellular dolomites, evaporites and limestones that were deposited on a marine shallow shelf with interval bound terrigenous input (Gruber et al., 2022; Jerz, 1966; Krainer et al., 2011; Sausgruber, 1994a). Compared to the underlying Middle Triassic carbonate platform, the Raibl beds form a relatively incompetent succession. Norian dolomites (The increased eradication of ripple marks and intercalated shale horizons marks the transition between the Raibl beds and the overlying Hauptdolomit carbonate platform) (Fruth & Scherreiks, 1982; Müller-Jungbluth, 1968; Zorlu, 2007), forming the second major platform of the NCA. Lithologies consist of inter- to supratidal, laminated dolostone and subtidal dolo-mudstones form the second major platform of the NCA, which is again 1-2 km thick (Donofrio et al., 2003), which contain scarce fossils. The early evolution of the Hauptdolomit platform is characterized by local anoxic basins, represented in the stratigraphic succession by bituminous intervals and coaly shales . Sedimentary textures typical for a supra- to intertidal lagoonal depositional environment occur in the middle level of Hauptdolomit .The Hauptdolomit platform subsequently drowns towards its top; a Norian succession of alternating limestones and dolostones (Plattenkalk; Gümbel, 1861)the alternation of limestone and dolomite in the upper Hauptdolomit succession gradually evolves into the well bedded and fossiliferous Plattenkalk limestone (Norian) heralds the deposition of Rhaetian basinal shales (Kössen Fm),. Together, Hauptdolomit and Plattenkalk show a thickness > 1000 m in the Achensee region . Further drowning resulted in the deposition of the subtidal Kössen Fm (Norian-Rhaetian) , marked by increasing intercalated marls and shales , which interfinger with Upper Rhaetian platform carbonates (Oberrhät limestone; Golebiowski, 1991; Riedel, 1988) (Figure 32).

The Ladinian and Norian platforms represent an approximately 3 km thick, mechanically competent unit. The mechanical significance of intervening Carnian shales and evaporites for deformation during the Cretaceous orogeny has been previously discussed (Kilian et al., 2021) and approached through analogue modelling in this contribution (see Section 3.2 and 4 below).

While rifting of the Alpine Tethys (Eberli et al., 1993) in the Jurassic caused subsidence and drowning of the Triassic carbonate platforms (Ortner et al., 2008), rotational block faulting caused by the extensional movement (Lackschewitz et al., 1991) resulted in a differentiation of basin and swell facies (Nagel et al., 1976; Spieler & Brandner, 1989). Early Jurassic red condensed limestones (e.g., Adnet Fm, Sinemurian–Toarcian; Sausgruber, 1994a; Spieler, 1994)Hierlatzkalk;) containing manganese nodules were deposited on swells, and basinal strata (e.g., Scheibelberg Fm., Hettangian-Toarcian; Allgäu Fm. Hettangian–Oxfordian) in subsided areas (Brandner & Gruber, 2011: Fig. 15).). Gravitational scarp fault breccias and debris flows are intercalated in the basinal slope specular limestones of the Scheibelberg Fm and the interfingering, more distal Allgäu Fm (Spieler & Brandner, 1989). The local bBasins and swells differentiation and sedimentation was preserved existed until the Middle-Late Jurassic (Brandner & Gruber, 2011; Ortner et al., 2008; Ortner & Kilian, 2016; Spieler & Brandner, 1989). The continental margin reached its maximum subsidence in the Oxfordian (Ortner & Kilian, 2016), when the Ruhpolding radiolarites were deposited (OxfordianRuhpolding radiolarite) (Bernoulli & Jenkyns, 1974; Nagel et al., 1976; Sausgruber, 1994a) as one of the deepest lithofacies of the Tethys was deposited. The overlying Late Jurassic-Early Cretaceous (Kimmeridgian-Berriasian) stratigraphic succession (e.g., Tauglboden Fm, Ammergau Fm, Oberalm and Schrambach FmsFm, Barmstein limestones) testifies to a shallowing depositional environment (Gawlick, 2004; Gruber et al., 2022; Gümbel, 1861; Kilian, 2013; Lipold, 1854; Sausgruber, 1994a). The lower–middle Jurassic succession (Scheibelberg Fm-Tauglboden Fm) has a mean thickness of 290 m (based on cross

sections and compilations of Auer, 2001; Gruber, 2011; Ortner & Gruber, 2011; Sausgruber, 1994b; Spieler, 1995), while the upper Jurassic to lower Cretaceous pelagic limestones (Oberalm Fm) reach a thickness of more than 1300 m and cover the pre-existing relief (Nagel et al., 1976). The Ammergau Fm (Kimmeridgian-Tithonian) has a mean thickness of 309 m and the Oberalm Fm (Tithonian-Berriasian) has a mean thickness of 1075 m.

An iIncrease influx of in siliciclastic detritus, beginning in the Early Cretaceous, marks the onset of synorogenic sedimentation, commencing with the Schrambach Fm (Berriasian-Aptian), consisting of marls and intercalated calcareous and turbiditic sandstones (Lipold, 1854; Ortner, 2003a). In the western Thiersee syncline, its thickness is ~ 300-400 m (Ortner & Gruber, 2011; K.-I. Schütz, 1979), thinning to ~ 150 m east of Achenkirch (Ortner & Gruber, 2011). The overlying synorogenic sediments of the Gosau Group (Late Cretaceous to Paleogene) complete the stratigraphic succession of the Achental structure regionand Northern Calcareous Alps (Ortner, 2003a).

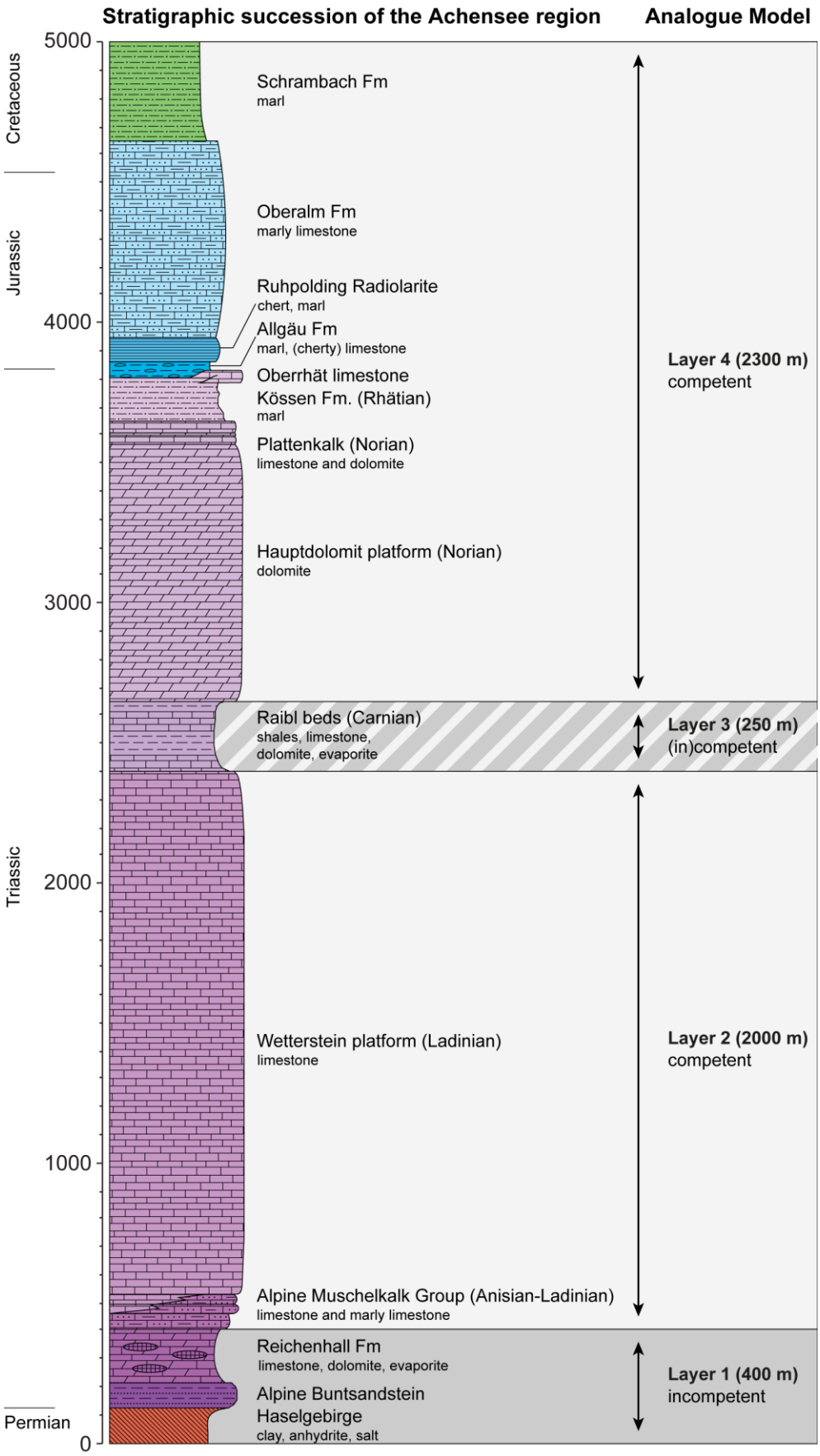
Stratigraphic succession of the Achensee region
Analogue Model
5000
4000
3000
2000
1000
0
Cretaceous
Jurassic
Triassic
Permian
Schrambach Fm
marl
Oberalm Fm
marly limestone
Ruhpolding Radiolarite
chert, marl
Allgäu Fm
marl, (cherty) limestone
Oberrhät limestone
Kössen Fm. (Rhätian)
marl
Plattenkalk (Norian)
limestone and dolomite
Hauptdolomit platform (Norian)
dolomite
Raibl beds (Carnian)
shales, limestone,
dolomite, evaporite
Wetterstein platform (Ladinian)
limestone
Alpine Muschelkalk Group (Anisian-Ladinian)
limestone and marly limestone
Reichenhall Fm
limestone, dolomite, evaporite
Alpine Buntsandstein
Haselgebirge
clay, anhydrite, salt
Layer 4 (2300 m)
competent
Layer 3 (250 m)
(in)competent
Layer 2 (2000 m)
competent
Layer 1 (400 m)
incompetent

Figure 3: Stratigraphic overview of the Permian–Cretaceous sedimentary succession of the Karwendel thrust sheet in the Achensee area. ~~Compilation of data from , and .~~Modified after Kilian et al. (2021).

2.2 Achental structure

The Achental structure is located within the Karwendel thrust sheet ~~of the NCA~~, following the revised nappe structure of the NCA (Kilian & Ortner, 2019; Ortner, 2016; Ortner & Kilian, 2022), and geographically surrounds ~~Lake Achen (German:~~ the Achensee~~)~~ in Tyrol, Austria (Figures 1, 4). ~~The nappe structure of the NCA has recently been revised . Consequently, the former Inntal and Lechtal thrust sheets have been combined in the Karwendel thrust sheet (Figure 1a), which overthrusts the Tannheim thrust sheet (combined from the Allgäu thrust sheet, Puitentalzone and Karwendelschuppenzone) to the north .~~The structure is characterized by the low-angle Achental thrust, which separates the Karwendel and Thiersee synclines in its footwall, from the Guffert-Unnutz-Montscheinspitze anticline fold train in its hanging wall. ~~The Achental structure~~It forms a structural NNE-SSW striking transfer zone between Karwendel and Thiersee synclines~~., with t~~The Achental thrust ~~reaching~~ reaches into the cores of these folds and gradually lose~~s~~~~ing~~ offset toward the NE and SW (Ortner & Gruber, 2011). The thrust changes its orientation and stratigraphic offset throughout the Achental structure; in the north (Mahmooskopf-Natterwand section, Figure 4), the thrust strikes E-W and dips ~ 23-30° south (Ortner, 2003a and Beer, 2003, respectively) with a total displacement of ~ 5-7 km (Auer & Eisbacher, 2003 and Ortner, 2003a, respectively), based on cut-offs of Jurassic strata in Section B (Figure 5b). In the central section, the thrust strikes NNE-SSW and dips 15° SE (Spieler, 1994). ~~It reaches a~~The maximum stratigraphic offset of ~ 8 km (Eisbacher & Brandner, 1996) is located NE of Achenkirch, where Hauptdolomit (Norian) is thrusted onto Schrambach Fm (Early Cretaceous) (Figures 4, 5a) (Gruber et al., 2022). In the south, the Achental thrust dips SE, offsets the hinge of the Seebergspitze syncline and runs into the core of the Karwendel syncline (Figure 4). ~~Although here the thrust~~ Although it separates consecutive Late-Jurassic-Early Cretaceous strata, the contrasting orientation of the strata (E-dipping north of the Seebergspitze syncline hinge; vertical to S-dipping west of the hinge) rules ~~the SE dip of the thrust is strongly opposed to the steep E- to SE dip of the strata, ruling~~ out a stratigraphic contact between these formations (Ortner & Gruber, 2011). However, offset is minor and and dies out not much further to the west. A series of km-scale, E-W striking north-vergent synclines (~~The~~ Karwendel, ~~Scharfreuter,~~ Gröben, ~~and~~ Großzemmalm, Klammbach and Thiersee synclines) and ~~the~~ associated anticlines (Scharfreuter and Hofjoch anticlines) ~~and Klammbach syncline~~ form the footwall of the Achental thrust (Figure 4). These ~~are km-scale, E-W striking north-vergent~~ folds ~~that are overturned to recumbent, and~~ are overridden by the Achental and Leiten thrust ~~and its associated faults~~ (~~e.g., Leiten thrust;~~ Ortner & Gruber, 2011: their Figure 2). ~~The recumbent Thiersee syncline forms the north vergent eastern continuation of the Klammbach syncline .~~

The hanging wall of the Achental thrust ~~is referred to as the~~ ("Achentaler Schubmasse" after Quenstedt (1933)~~) . It~~ is comprised of the connected Montscheinspitze, Unnutz and Guffert anticlines (Figures 4, 5), which change strike approximately parallel to the Achental thrust. West of the Achental structure, the Montscheinspitze anticline is connected to the Karwendel syncline (Ampferer & Heissel, 1950: their section 3). In the SW corner of the Achental structure, the northern anticline limb is folded with the Seebergspitze syncline into an overturned position (Fuchs, 1944; Ortner & Gruber, 2011). The Achental thrust emplaces the anticline limb ~~and thrusted~~ onto the Karwendel syncline ~~along the Achental thrust~~ (Nagel et al., 1976). The ~~Montscheinspitze anticline then continues toward the north as the~~ Unnutz anticline, ~~which is~~ a recumbent fold with a SE-dipping axial surface and an increasingly SSW-plunging fold axis (From N-S 205/18, 200/27 and 187/23; Ortner & Gruber, 2011), forms the N-S striking part of the fold train. The Unnutz anticline (Figure 5a) resembles a dome, rather than a cylindrical fold (e.g., Mojsisovics, 1871; Ortner & Gruber, 2011; Sausgruber, 1994a, 1994b) ~~with an upright limb that changes strike from E-W to NE-SW~~. NE of Achenkirch, the Unnutz anticline is folded around the ~~Steigwand anticline and~~ Rotmöserkopf synform and continues as the E-W

striking Guffert anticline (Gruber et al., 2022; Ortner & Gruber, 2011) (Figures 4, 5b). The Guffert anticline has a S-dipping axial surface, sub-horizontal fold axis with ESE-WNW strike and ~~shows~~ an overturned northern limb.

The characteristic sigmoidal shape of the ~~resulting~~ Guffert-Unnutz-Montscheinspitze anticline fold train ~~in the Achentaler Schubmasse forms a characteristic sigmoidal shape that~~ has been noticed since the beginning of the 20th century (Ampferer, 1902) and is one of the greatest complexities in the geologic interpretation of the Achental structure. Over the past century, four principal hypotheses have been developed to explain ~~the~~ its formation ~~of this sigmoidal fold train~~ (see also Ortner & Gruber, 2011; Gruber et al., 2022). These include *1)* bending of an originally E-W striking anticline due to rotational movements~~, forming the N-S striking Unnutz anticline as a central segment~~ (e.g., Ampferer, 1921, 1941; Auer, 2001; Spengler, 1953, 1956); *2)* passive dragging of the central part of the structure, caused by a larger amount of shortening in the eastern part of the structure, compared to its western part (Nagel, 1975); *3)* polyphase deformation, in which a former W-directed thrust (Achental thrust) was reactivated by N-directed thrusting (Channell et al., 1990; Channell et al., 1992; Fuchs, 1944; Ortner, 2003a; Spieler & Brandner, 1989), and *4)* forced folding of the Guffert-Unnutz-Montscheinspitze fold train at the border of a carbonate platform, or along an inverted Jurassic normal fault (Eisbacher & Brandner, 1995, 1996; Ortner & Gruber, 2011).

~~In accordance with the third hypothesis, t~~The kinematic history of the Achental structure ~~has been affected~~is characterised by polyphase shortening (Fuchs, 1944; Ortner, 2003a; Ortner & Gruber, 2011; Spieler & Brandner, 1989)~~, beginning in the Early Cretaceous with the formation of the Guffert anticline~~. Barremian sediments below the Achental thrust indicate an Early Cretaceous maximum age of thrusting. ~~Both the Achental and Leiten thrust are folded with the E-W striking Roßstand anticline, but not with the parallel Scharfreuter anticline (their Fig. 2) (Figure 3). Folding of the Achentaler Schubmasse around these folds suggests that the Achental thrust is older than the general N-directed shortening.~~ The oldest contractional deformation in the area is indicated by an angular unconformity in both limbs of the Guffert anticline at the base of the Gosau Group ~~15 km east of the Achental structure~~ (Ortner & Gruber, 2011), indicating Early Cretaceous growth of the anticline. Anticlines grow on top of décollements, and we speculate that the Achental thrust was already active. ~~However, since the oldest sediments covering both the hanging wall and footwall of the northern Achental thrust belong to the Gosau Group, N-directed shortening must have occurred post-Gosau, post-dating the formation of the western Achental thrust.~~ Cretaceous shortening along the Achental thrust is evident from calcite slickensides showing NNW- to NW-directed movement ~~along the Achental thrust~~ (Eisbacher & Brandner, 1995, 1996; Sausgruber, 1994a, 1994b)~~, based on calcite fibre lineations~~. This phase of shortening caused an initial uplift and tightening of the Unnutz-Achental structure and is responsible for NW-striking high-angle dextral transfer faults, which segment the Unnutz anticline (Eisbacher & Brandner, 1995, 1996). ~~In contrast,~~ Late Cretaceous to Paleogene (80-30 Ma) NE-directed shortening superimposed existing folds and fault movement, reactivating pre-existing NW-striking transfer faults and forming NW-plunging folds and NE-striking high-angle transfer faults (Eisbacher & Brandner, 1995). As a result, three major fold orientations are recognized in the Achensee region (Sausgruber, 1994a). Folds with NE-SW striking fold axes formed during NW-directed, pre-Gosau contraction. E-W striking fold axes formed during N-directed shortening and NW-SE striking fold axes formed during NE-directed shortening. Folding of the Achental and Leiten thrust around the E-W striking Roßstand anticline, but not around the parallel Scharfreuter anticline (Sausgruber, 1994b; Ortner & Gruber, 2011: their Fig. 2) (Figure 4) suggests that the thrust is older than the general N-directed shortening (Spieler & Brandner, 1989). However, since the oldest sediments covering both the hanging wall and footwall of the northern Achental thrust belong to the Gosau Group, N-directed shortening must have occurred post-Gosau (Ortner, 2003a), post-dating the formation of the western Achental thrust. Neogene folds superimpose older folding and can be found e.g., within the Thiersee syncline (Sausgruber, 1994b). ~~In general, f~~Fold interference creates intriguing dome-and-basin structures that complicate the geological interpretation of the Achental structure. ~~Although p~~Polyphase deformation of the Achental

structure is visible from field evidence, showing refolded faults and fold axes (e.g., Gruber et al., 2022; Ortner & Gruber, 2011; Sausgruber, 1994b).~~,~~ However, it is unclear whether ~~has not been proven that~~ two phases of deformation were necessary to create the Achental structure (Gruber et al., 2022).

~~Following the fourth hypothesis, several studies propose a~~A link between ~~a~~ the Jurassic basin architecture and the present-day sigmoidal form of the Achental structure has been proposed previously, suggesting that the latter is the result of forced folding (Eisbacher & Brandner, 1995, 1996; Ortner & Gruber, 2011) that depended on pre-existing extensional structures rather than the exact direction of shortening (Töchterle, 2005). Channell et al. (1990) postulated the existence of an E-W striking sinistral pull-apart basin, forming a ~~The existence of a~~ controlling inherited Jurassic basin-and-swell topography. This is supported by field observations. Cretaceous transport directions (Ortner & Gruber, 2011; Sausgruber, 1994a, 1994b) are oblique to the axis of the Karwendel and Thiersee synclines. If deformed within a single episode of shortening, this requires pre-existing faults for localization of folding and thrusting. Furthermore, the thickness of Jurassic deposits differs in both limbs of the Karwendel and Thiersee synclines (Nagel et al., 1976) and the maximum sedimentary thickness of Upper Jurassic strata is located in the overstep area between the two synclines (Figure 1b). The strata show ~~is supported by~~ a clear facies differentiation and a generally~~n~~ increasing thickness of basinal Jurassic strata, from 100 m near Mittenwald (30 km W of the study area) to 1100 m in the Bächental (10 km NW of the study area; e.g., Gruber et al., 2022; Nagel et al., 1976; Ortner & Kilian, 2016; K.-I. Schütz, 1979; Ulrich, 1960) (Figure 1b), showing an increased subsidence toward the SE end of the Karwendel syncline. This suggests that a basin existed that was bound by normal faults at a high angle to the faults in the synclines. Since major normal faults have not been mapped east of the Achental thrust, we interpret a W-dipping blind fault controlling deposition and facies differentiation in the Jurassic. Pliensbachian and Toarcian mass-flow sediments and scarp-breccias that are found near the basin slopes (Spieler & Brandner, 1989) support this hypothesis. Based on the aforementioned, it~~The Jurassic extensional basin-and-swell topography~~ was proposed that this Jurassic basin-and-swell topography, in the form of~~o form the foundation of the present-day Achental structure, in which~~ a N-S to NE-SW striking pull-apart basin (Ortner & Gruber, 2011; Spieler & Brandner, 1989) or negative flower structure (Sausgruber, 1994b) ~~was~~ bordered by E-W striking sinistral strike-slip faults, forms the foundation of the present-day Achental structure. We therefore use this basin geometry as the base for our analogue models. ~~This is supported by Pliensbachian and Toarcian mass-flow sediments and scarp-breccias that are found near the basin slopes.~~

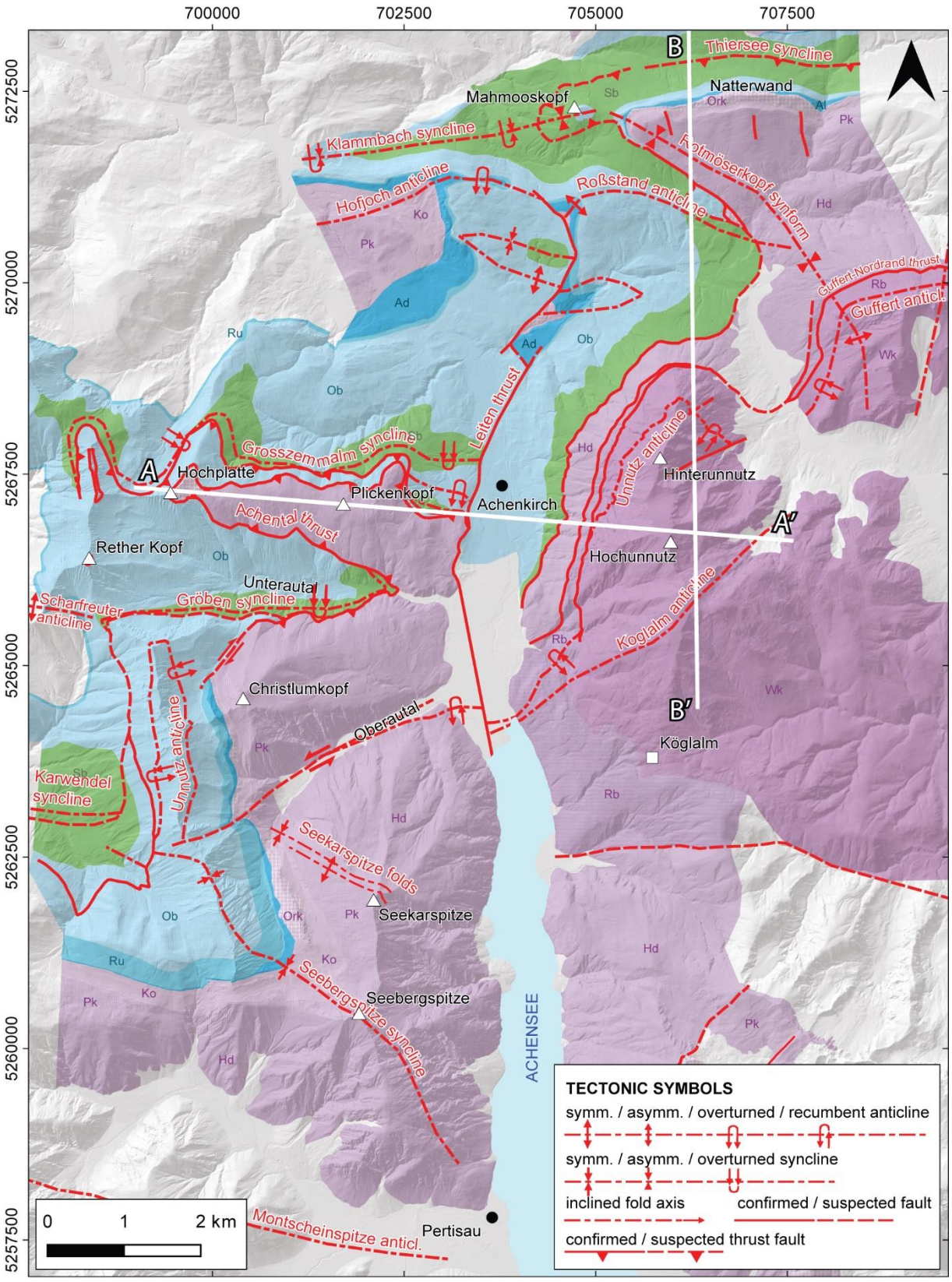

TECTONIC SYMBOLS

symm. / asymm. / overturned / recumbent anticline

symm. / asymm. / overturned syncline

inclined fold axis

confirmed / suspected fault

confirmed / suspected thrust fault

LITHOLOGIES

Sb	Lower Cretaceous marl (Schrambach Fm)	Ork	Rhaetian limestone (Oberrhätkalk)
Ob	Upper Jurassic limestone (Oberalm Fm)	Ko	Rhaetian marl (Kössen Fm)
Ru	Oxfordian radiolarite (Ruhpolding r.)	Pk	Norian lime- and dolostones (Plattenkalk)
Ad	Lower-Middle Jur. condensed limestone (Adnet Fm)	Hd	Norian platform (Hauptdolomit)
Al	Lower-Middle Jurassic limestone (Allgäu Fm)	Rb	Carnian shales, evaporites and carbonates (Raibl beds)
		Wk	Ladinian platform (Wetterstein limestone)

Figure 4: Geological map of the Achental structure compiled from Sausgruber (1994b), Spieler (1995), Auer (2001), Gruber (2011) and own data. Modified after Ortner and Gruber (2011). Sections A-A' and B-B' are shown in Figure 5.

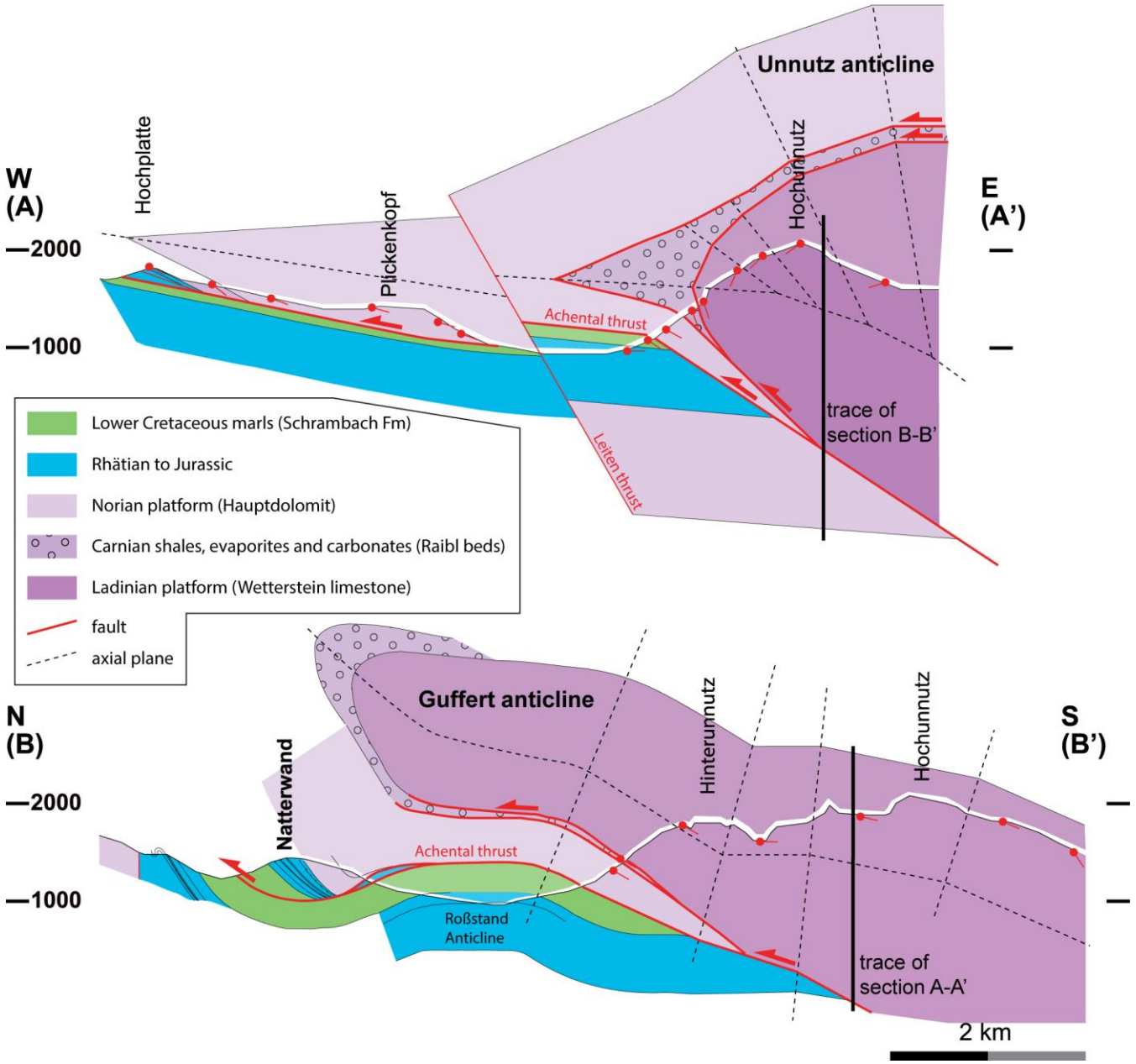

Figure 5: Cross sections (a) of the Unnutz anticline (Section A-A') and (b) of the Guffert anticline (Section B-B'). Section traces are marked in Figure 4. Modified after Ortner (2003a).

3 Analogue modelling

3.1 Modelling strategy

Regional-scale physical analogue modelling was conducted to investigate the influence of pre-existing basin-bounding extensional faults on oblique basin inversion, within the geological framework of the Achental structure. The goals of the experiments included testing 1) the importance of a weak basal décollement, 2) the influence of thick-skinned versus thin-skinned tectonics, and 3) the role of pre-existing structures in deformation localisation. Geological parameters from the natural example form the basis for our modelling approach. When translating geological structures into analogue models, a number of details and complexities are

inevitably omitted, resulting in the creation of a simplified modelling basis that incorporates only the most important elements. In the case of the Achental structure, we have chosen to use the predicted Jurassic fault and basin geometry as a modelling basis, with a W-dipping normal fault and two E-W striking strike-slip faults. This is comparable to the basin geometry proposed by e.g., Ortner and Gruber (2011) and Spieler and Brandner (1989), and is based on facies and thickness changes within Jurassic deposits, as well as structural considerations outlined in Section 2.2. The rheological properties of the NCA sedimentary succession, described in Section 2.1, were considered for the layering of the analogue models. For the basal Permo-Triassic Haselgebirge-Reichenhall succession we used ductile modelling materials (layer 1; Figures 3, 6). The middle and upper Triassic carbonate platforms are represented by brittle materials (layers 2 and 4). Rhätian to Lower Cretaceous units are largely marls and marly limestones (Figure 3). Although these are considered less competent units than the Ladinian and Norian platform carbonates, they are on the top of the analogue model and do therefore not control the modelling result. The Carnian Raibl beds were modelled using brittle or ductile materials, depending on the specific model (layer 3; Figure 6). Analogue models were set up to simulate the~~show an increasing~~ lithological and structural ~~likeness~~ configuration of~~to~~ the eastern margin of the Jurassic Achental basin, resulting in an increasing model complexity.

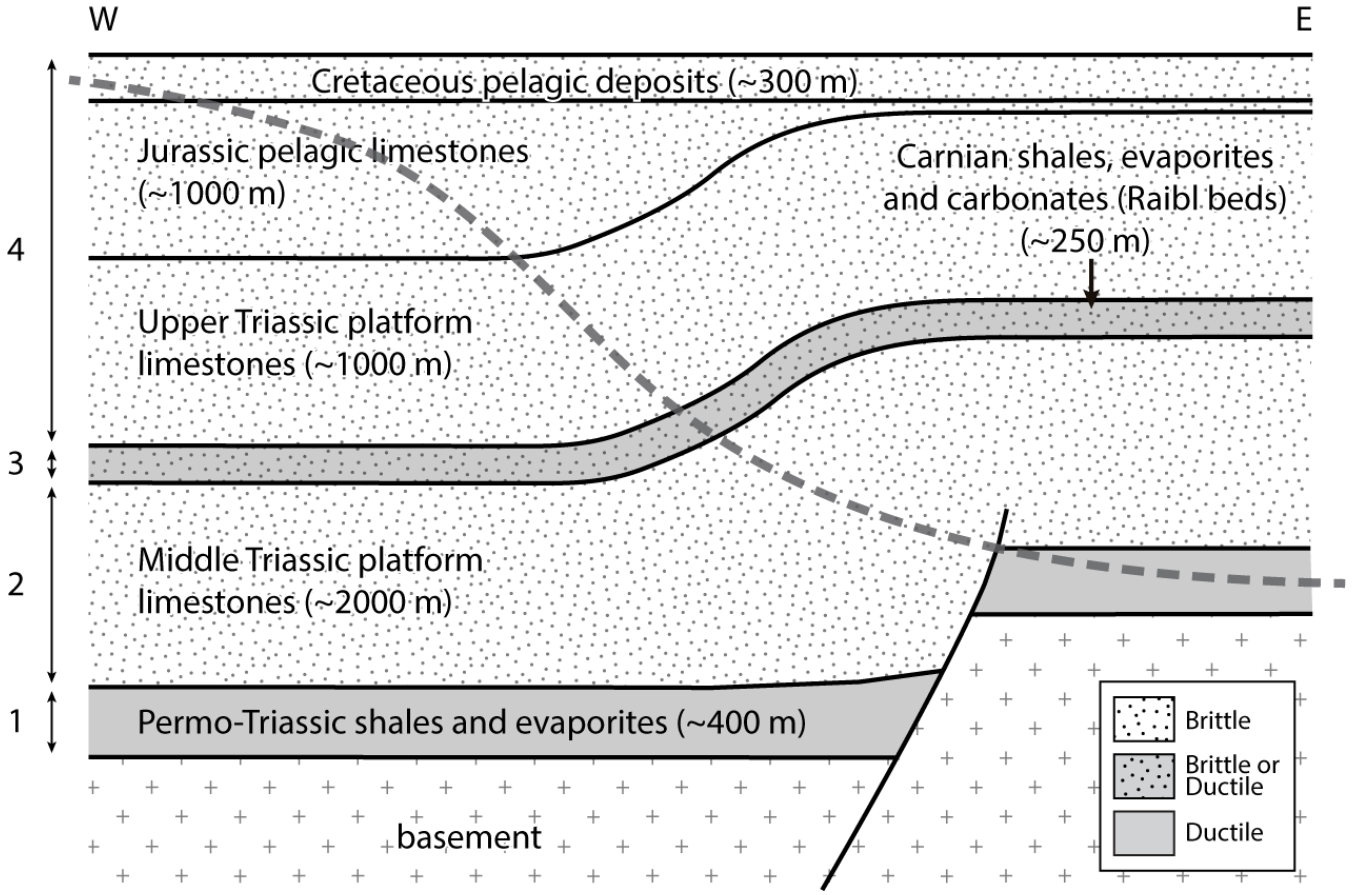

Figure 6: Schematic diagram showing the geological set-up of the eastern margin of the Achental basin, prior to inversion. ~~Grey bold~~Dashed line represents inversional trace of the Achental thrust. Lithologies are marked brittle or ductile, depending on their mechanical properties.

3.2 ~~Geometric and kinematic~~Modelling setup

Brittle and ductile modelling materials represent different parts of the NCA and Tethyan stratigraphy (Figure 3). A ductile layer of ~ 400 m thick, incompetent evaporites and shales, forming the basal décollement of the NCA was represented by silicone putty in models, with a thickness of 0.4 cm (Figures 6, ~~and~~ 7a). The silicone putty is a mixture of RBG-0910 Dow Corning silicon polymer

and ~~fine~~ iron powder (~ 32 wt.%) with a density of ~ 1360 kg m^{-3}. We determined a viscosity (η) of 20456 Pa s for the modified silicone putty, using a coni-cylindrical viscometer under room temperature (21 ± 1 °C) (Lee & Warren, 1940; Mooney & Ewart, 1934, see also Willingshofer et al., 2005). The viscosity of natural evaporites, albeit highly variable, is estimated to be 10^{19} Pa s (Allen & Beaumont, 2016; Weijermars, 1986a, 1986b, 1986c; Weijermars et al., 1993; Weijermars & Schmeling, 1986), resulting in a viscosity scale ratio of 2.046 · 10^{-15}. The ~~modified~~ silicone putty exhibits near-Newtonian behaviour and has an n-value of 1.27 in laboratory tests. The predominantly carbonatic, brittle sedimentary cover of the NCA was represented by dry quartz sand (Figure 6), a Mohr-Coulomb material, with a density of ~~1510~~ 1500 kg m^{-3} (e.g., Willingshofer et al., 2018). The quartz sand was sieved on top of the silicone putty, to create a total model thickness of 5 cm (Figure 7a). The density of the natural prototype was approximated by the density of Triassic Muschelkalk, ~~and amounts to~~ which is ~ 2680 kg m^{-3} (Manger, 1963: p. E31), ~~so that~~ resulting in a density ratio (ρ*) of 0.56 between model and nature ~~exists~~. An intermediate layer of Upper Triassic carbonatic-evaporitic strata (Raibl beds) was modelled as either brittle or ductile layer, depending on the model-specific set-up (Figure 7a-b). For a discussion whether this unit behaves incompetent or not, see Kilian et al. (2021). Assuming that inertial forces can be neglected in the analogue models (see discussion in Del Ventisette et al., 2007; Wickham, 2007), the scaling of time and length is allowed to deviate from the principle of dynamic similarity and their "ratios can be considered as independent variables" (Dombrádi et al., 2010, p. 109). The principles of dynamic, geometric and rheological scaling are discussed in Hubbert (1937), Ramberg (1981), Weijermars and Schmeling (1986), Merle and Abidi (1995), Brun (1999), Sokoutis et al. (2000; 2005) while their relationships between model and nature are summarized in Table 1.

Table 1: Summary of model parameters. Experimental material parameters from Willingshofer et al. (2005; 2018). For strength envelops, see Figure 7b.

Materials/parameters		**Model**	**Nature**	**Ratio (m/n)**
Brittle layer	Thickness	Max. 0.05 m	Max. 5000 m	10^{-5}
(Quartz sand)	Density	~~1510~~ 1500 kg m^{-3}	2680 kg m^{-3}	0.56
	Strength	Max. 1471.5 Pa	Max. 2.63 · 10^{-8} Pa	5.597 · 10^{-6}
Ductile layer	Thickness	0.004 m	400 m	10^{-5}
(Silicone mixture)	Density	1360 kg m^{-3}	2450 kg m^{-3}	0.56
	Viscosity	20456 Pa s	10^{19} Pa s	2.046 · 10^{-15}
	Strength	28.41 Pa	2550933 Pa	1.11 · 10^{-5}
	n-value	1.27		
Length				10^{-5}
Strain rate		2.77778 · 10^{-6}~~0.01~~ m/~~h~~s	1.02422628 · 10^{-10} ~~0.00323~~ m/~~yr~~s	27137
Time		288008 ~~3960011 h~~s	7.8146208 · 10^{13} ~~2.478~~ 1.0747469 · 10^{-14} ~~3.408 Ma~~s	3.685 · 10^{-10}
Bulk shortening		0.08–0.11 m	8000–11000 m	10^{-5}

Model materials were placed in a rectangular fault box with metal bars as sidewalls and a wooden piston of 40 or 83 cm width as a moving wall (Figure 7c). We chose a length scale-ratio (L*) of 10^{-5}, so that 1 cm in the model represents 1 km in nature (Table 1). In all experiments, a pre-existing normal fault, similar to the boundary fault of the Achental basin was represented by a rigid basal plate (footwall block) with a 60° dipping ramp (fault plane). In model-specific set-ups, the direction of shortening (at 90 or 45° to the ramp), the movement of the basal plate (fixed or mobile) and the layering sequence of the model (Figure 7a) were varied (Table 2). Shortening at 90° to the ramp represents the simplest possible scenario, whereas shortening at 45° to the ramp reflects oblique shortening during Cretaceous shortening. Moving the basal plate with the brittle-ductile materials on top represents thick-skinned shortening, whereas a fixed basal plate with movement only in the cover reflects thin-skinned shortening of the NCA. A varying layering with zero, one or two décollements tests the importance of a weak basal décollement and decoupling at the base or within the sedimentary cover. The modelling strategy evolved from a basic brittle model ~~set-up~~(A) using the simplest geometric, kinematic and lithological parameters possible. The same model set-up ~~, which~~ was then applied to ~~one brittle (A1) and three~~ brittle-ductile (B1-B3) models. The set-up featured a basal plate with dimensions of 40 x 22.5 cm, a thickness of 1 cm and a 60° dipping front ramp (Figure 7), representing the Jurassic normal fault. A wooden piston of 40 cm width was placed behind (A~~1~~, B1) or on top of (B2, B3) the basal plate, so that the plate was either mobile or fixed, exemplifying the effect of thick- versus thin-skinned tectonics. Shortening was applied at 90° to the front ramp with a convergence rate of 8 cm/h for the brittle model (A~~1~~) and 1 cm/h for the brittle-ductile models (B1-B3), and a total shortening of 8 cm (Table 1). The convergence rates between brittle and brittle-ductile models vary, because the strength of the ductile material depends on e.g., the strain rate, whereas this is not the case for brittle materials. For the brittle model, only quartz sand was used as a modelling material. In the brittle-ductile models, a basal layer of silicone putty was placed on top of the basal plate (B1, B3) or over the basal plate, ramp and table top (B2). For technical reasons model B1 (and, for comparison, model B3) do not have silicone putty on the table top, because the material may stick beneath a mobile basal plate, creating modelling artefacts. Model set-ups with a fixed basal plate do not have this problem. A small amount of dishwashing soap was spread between the plate and the silicone putty, to prevent sticking ~~increase the décollement function~~ of the ductile layer to the substrate. Model B2 featured an additional, upper ductile layer (Figure 7a), representing incompetent behaviour of the Carnian Raibl beds (Figures 3, 6).

For model C~~1~~ we added two plates to the north and south of the ~~fixed~~ main basal plate, to simulate E-W striking strike-slip faults and expected sigmoidal fault arrangement in the subsurface of the ~~bounding the~~ Achental ~~basin~~structure. This required the use of a piston with a width of 83 cm. The basal plates were fixed, representing a thin-skinned style of deformation. Shortening remained orthogonal to the ramp at 1 cm/h, but total shortening was increased to 11 cm to accommodate the larger size of the model set-up. The basal ductile layer of silicone putty was placed on top of the basal plates and on the table top, but was disconnected at the ramp (Figure 7) to create a clear velocity discontinuity as seen in model B3.

For models D1 and D2 the fixed main basal plate and two auxiliary plates were rotated 45°, to simulate Cretaceous oblique shortening at 45° to the ramp (Jurassic normal fault). We applied a total shortening of 11 cm, identical to model C. For both models, the basal ductile layer was placed on the basal plate and table top, while being disconnected at the ramp to create a ~~clear~~ velocity discontinuity as in model C (see e.g., Allemand & Brun, 1991; Tron & Brun, 1991). M~~, but m~~odel D2 featured an extra, upper ductile layer, simulating incompetent behaviour of the Raibl beds, similar to model B2. ~~After reaching the desired shortening, models were covered with black sand for protection, drenched with water until saturation and left to rest for at least 2 hours. Sections were then cut orthogonal to the strike of major structures.~~

Table 2: Summary of modelling runs and relevant parameters.

Series		Layering	Silicone		Basal plate	Plate border	Angle (°)	Total shortening (cm)
			# Layers	At ramp				
A		Brittle	0	---	Mobile	Straigth	90	8
B	1	Brittle-ductile	1	Disconnected	Mobile	Straigth	90	8
	2	Brittle-ductile	2	Connected	Fixed	Straigth	90	8
	3	Brittle-ductile	1	Disconnected	Fixed	Straigth	90	8
C		Brittle-ductile	1	Disconnected	Fixed	Sigmoidal	90	11
D	1	Brittle-ductile	1	Disconnected	Fixed	Sigmoidal	45	11
	2	Brittle-ductile	2	Disconnected	Fixed	Sigmoidal	45	11

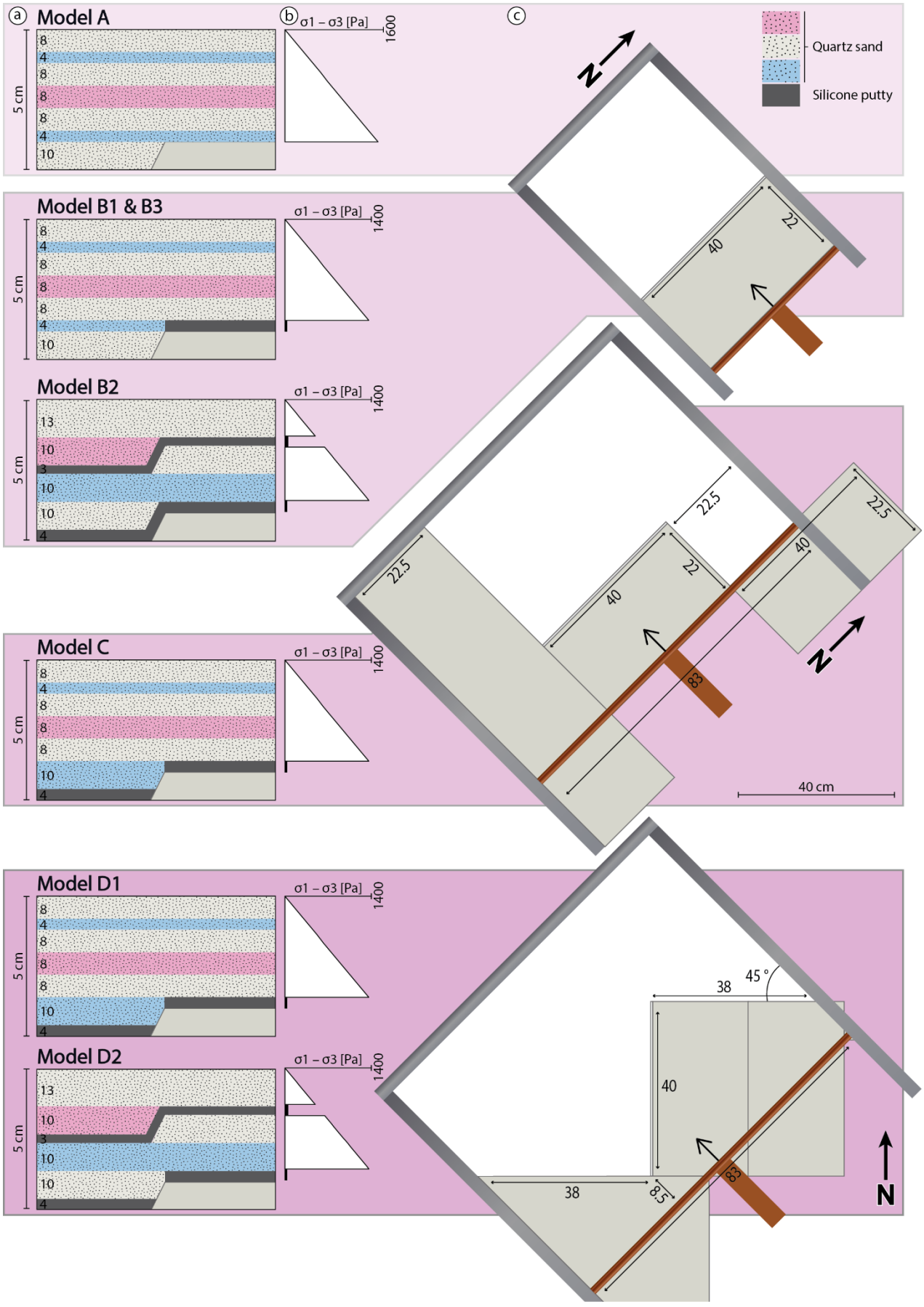
a
Model A
b
σ1 – σ3 [Pa]
1600
5 cm
8
4
8
8
8
4
10
c
Quartz sand
Silicone putty
N
Model B1 & B3
σ1 – σ3 [Pa]
1400
5 cm
8
4
8
8
8
4
10
40
22
Model B2
σ1 – σ3 [Pa]
1400
5 cm
13
10
3
10
10
4
22.5
22.5
40
22
40
22.5
83
N
Model C
σ1 – σ3 [Pa]
1400
5 cm
8
4
8
8
8
10
4
40 cm
Model D1
σ1 – σ3 [Pa]
1400
5 cm
8
4
8
8
8
10
4
45 °
38
40
Model D2
σ1 – σ3 [Pa]
1400
5 cm
13
10
3
10
10
4
38
8.5
83
N

Figure 7: Modelling set-up for model series A-D. (a) Layering sequences showing differently coloured layers of quartz sand and silicone putty with a total thickness of 5 cm. (b) Strength envelops showing strength (in Pa) of different modelling materials. (c) Basal plate set-ups showing the basal plate size (in cm).

3.3 Monitoring and model analysis

After reaching the desired shortening, models were covered with black sand for protection, drenched with water until saturation and left to rest for at least 2 hours. Sections were then cut orthogonal to the strike of major structures. Because these sections only show the final result and structure of the models, ~~P~~particle image velocimetry (PIV) was used to analyse incremental displacements in the analogue models (e.g., Leever et al., 2011; van Gelder et al., 2017), using powdered coffee grains on the model surface as markers. For all models, photographs of the top surface of the experiment were taken in a fixed time interval of 30 minutes. Photographs were then rectified to correct for lens distortion and processed using the MATLAB® vR2022a application PIVlab v2.57 (Thielicke, 2014; Thielicke & Sonntag, 2021; Thielicke & Stamhuis, 2014). In the image pre-processing settings, we enabled Contrast-Limited Adaptive Histogram Equalization (CLAHE) to locally enhance the contrast. FFT window deformation was used as the PIV algorithm. As post-processing steps we applied a velocity vector validation using a ~~standard deviation~~local median filter and interpolated missing data points.

The "strainmap" package (Broerse, 2021) for MATLAB® (vR2022a) was used for calculating cumulative strain type maps for models C and D1 based on incremental displacements from the PIV analyses. For a review of the underlying algorithms and practical applications of this software, see Broerse et al. (2021) and Krstekanić et al. (2021; 2022). Resulting colour-coded maps show the cumulative strain type (extension, strike-slip movement or shortening) at four points during the model runs (see figures in Section 4).

3.4 Limitations and simplifications

Similar to other analogue (and numerical) modelling studies, a measure of simplification is necessary to create a modelling basis from the natural example. Therefore, ~~O~~one of the major limitations of the experiments in this study is the necessary simplification of the initial fault configuration. The Jurassic basin-bounding faults are presently not exposed at the surface and thus their geometry and exact position are not known. It is assumed that the major present-day structural elements are aligned to the margins of the Jurassic Achental basin (Ortner & Gruber, 2011; Sausgruber, 1994b; Töchterle, 2005). Arguments for the existence of such a basin are presented in Section 2.2. Following the geometrical considerations for this basin~~Therefore~~, we chose a simplified~~e~~ subsurface~~initial~~ fault arrangement with one N-S and two E-W striking elements ~~was chosen~~ as the basis for the final series (C, D) of analogue models. Splay faults and additional basin-bounding faults are thus not considered here. The models were shortened in one single phase, simulating Cretaceous NW-directed shortening. However, the Achental structure was affected also by N-directed Paleogene and NE-directed Neogene shortening (Eisbacher & Brandner, 1995; Ortner & Gruber, 2011). These posterior phases of deformation were not taken into consideration for the analogue modelling, because they cannot explain the large offset along the Achental thrust in W–E sections (Ortner, 2003a; Ortner & Gruber, 2011) and are thus not expected to have created the main structural elements. The model set-up emphasizes the rheological contrast between a weak ductile basal décollement and a stronger upper brittle layer, whereas the characteristic, more complex heterogeneity of the NCA sedimentary cover was not included. Finally, the models ignore natural recovery processes such as erosion and sedimentation, which may influence the time–space evolution of structures. Eliminating limitations by increasing the complexity of models may increase the likeness between the analogue models and the natural example, but clouds the aim of analysing deformation localisation at pre-existing basin boundaries. Despite the~~se~~ simplifications described in this section, we are confident that our analoging~~ue~~ results are meaningful for the~~models were able to tackle the~~ problem under consideration~~and trace the large-scale deformation pattern as a response to compression~~.

4 Results

Model A is a purely brittle experiment with a maximum thickness of the sand layer of 5 cm. The piston pushed both the sand and the basal plate. In the initial stages of the experiment, an asymmetrical pop-up structure with a master back-thrust (1) and an antithetic fore-thrust (1) formed (Figure 8). ~~The master thrust is accompanied by a blind thrust that did not fully reach the surface.~~ Further shortening was accommodated by transient fore-thrusts (2, 6-8), which developed at the base of the ramp and migrated upward through the wedge, along the master back-thrust~~, with increasing shortening~~. ~~At 50% of total shortening, the frontal part of the wedge experienced gravitational collapse along a normal fault (4)~~.

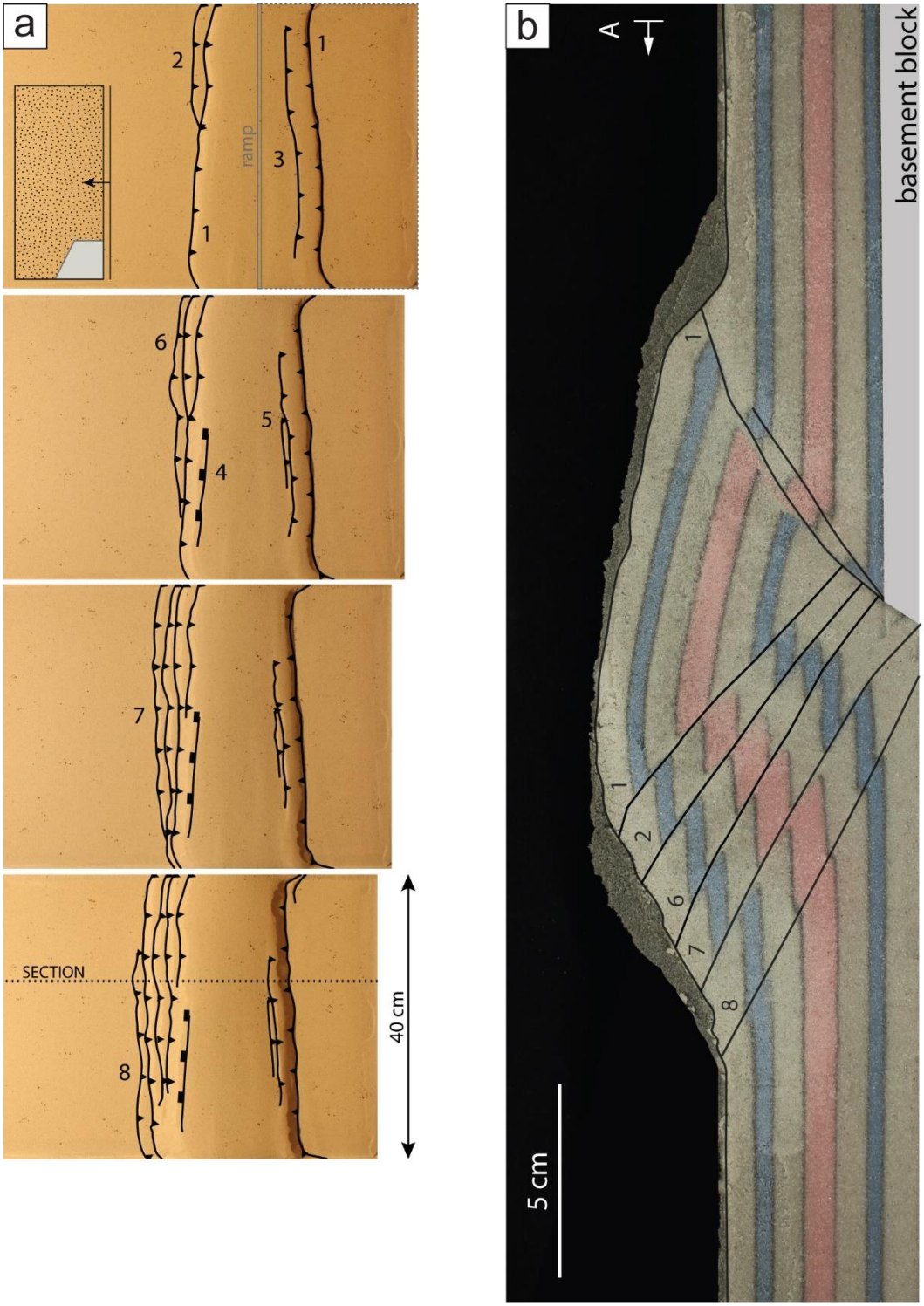

Figure 8: Modelling results of model A, showing (a) top views at 25, 50, 75 and 100 % of total shortening, and (b) side view at 100 % of total shortening. Location of section is marked in (a). Numbers show sequence of ~~initial~~ fault ~~activity~~formation. The inset in the first top view photograph shows the modelling setup in cross-sectional view.

Model B1-B3 (Figures 9,~~and~~ 10) ~~were set up similar to model A, but were designed as~~are brittle-ductile models with a basal ~~detachment~~ décollement of silicone putty, designed to study coupling and decoupling processes at the basal plate and ramp. Model B1 initially developed an asymmetric~~al~~ pop-up structure with an antithetic fore-thrust (1) and a master back-thrust (2) similar to model A (Figures 9a, 10a). ~~Shortening~~ Although shortening was initially accommodated equally along the back-thrust and the fore-thrust, ~~but final sections show that the~~ bulk shortening occurred along the master back-thrust. With further shortening, additional fore-thrusts (7, 9) form and ~~previously~~ former ~~active~~ thrusts migrate upward along the master back-thrust. All major thrusts originate from the velocity discontinuity at the ramp. Several secondary pop-up structures formed along splay faults (e.g., 3, 4, 6). The final resulting wedge is both wider and lower than in the brittle model A, and the internal wedge structure more complicated. ~~In m~~Model B2~~, we tested a different layering sequence with~~ contained an additional, upper ductile layer. Furthermore, the basal ductile layer was draped over the entire model base and connected at the mobile ramp~~, as opposed to model B1, where the silicone putty was placed only on the basal plate~~ (Figure 7a). During the first 25% of total shortening, a central wedge developed over the ramp, formed by two main back-thrusts separated at the upper layer of silicone putty. ~~Deformation shifted to the hinterland a~~At ~50% of total shortening~~, where~~ hinterland deformation created an asymmetrical pop-up structure with a main back-thrust ~~was formed~~ in the lower sand layers, and a symmetrical pop-up structure ~~was formed~~ in the upper sand layer above the upper ductile horizon. Pockets~~,~~ filled with air that was trapped underneath the silicone during model construction ~~and migrated during shortening, form~~ represent modelling artefacts. Overall, the height of the resulting wedge was far less than in model B1 and structures were mainly hinterland-oriented and dominantly backwards thrusting (Figures 9b, 10b). Thrusts ~~might~~ may have initially originated at the velocity discontinuity, but were laterally transported onto the mobile basal plate as shortening progressed. The upper and lower sand layer were completely decoupled at the upper silicone layer. For model B3 we used an identical layering as for model B1, but the basal plate was fixed simulating thin-skinned deformation~~and the piston was placed on top of the basal plate~~ (Figure 7). In the first half of the experiment (0-50% total shortening), a flip-type pop-up structure (see Smit et al., 2003, their Figure 4) with two back-thrusts and conjugate fore-thrust (1) developed directly in front of the piston (Figures 9c, 10c). Movement occurred along the main back-thrust, switched to the fore-thrust and back to the secondary back-thrust, as visible from lobes of silicone putty along the thrusts. At ~ 75% of total shortening, thrusting propagated into the foreland to form a strongly asymmetric pop-up structure with a master fore-thrust (5) and a minor back-thrust (6). The master thrust originated directly at the velocity discontinuity above the ramp. Although in the fixed plate scenario, as opposed to the mobile plate scenario, deformation did not localise directly above the ramp but rather required a wedge in the hinterland, the wedge geometry is much more asymmetric with most of the shortening occurring along a low-angle master fore-thrust that is antithetic to the original normal fault geometry.

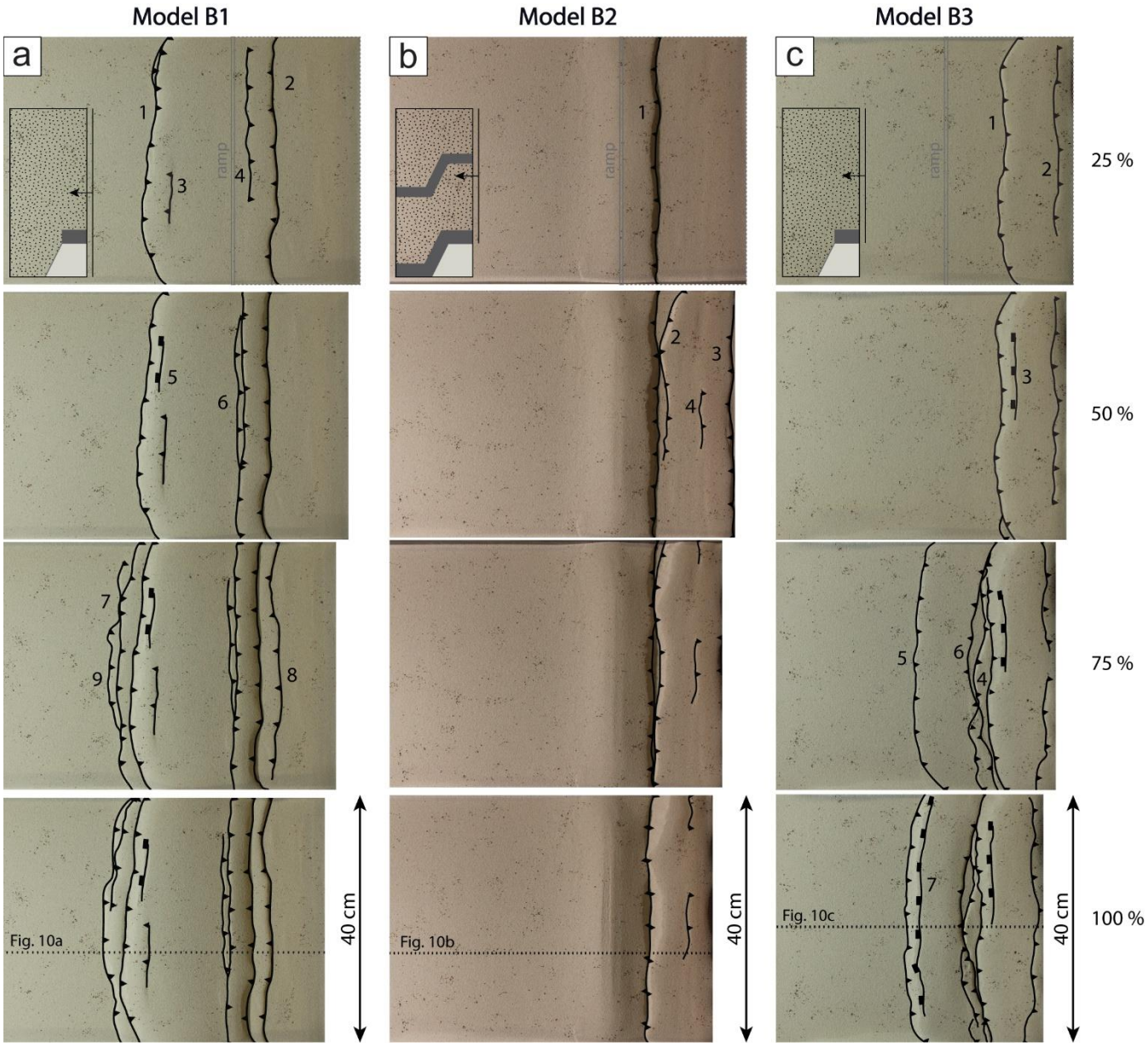

Figure 9: Top views of models (a) B1, (b) B2, and (c) B3 at 25, 50, 75 and 100 % of total shortening. Locations of sections are indicated (dotted lines). Numbers show sequence of ~~initial~~ fault ~~activity~~formation. The insets in the first top view photographs show the modelling setups in cross-sectional view.

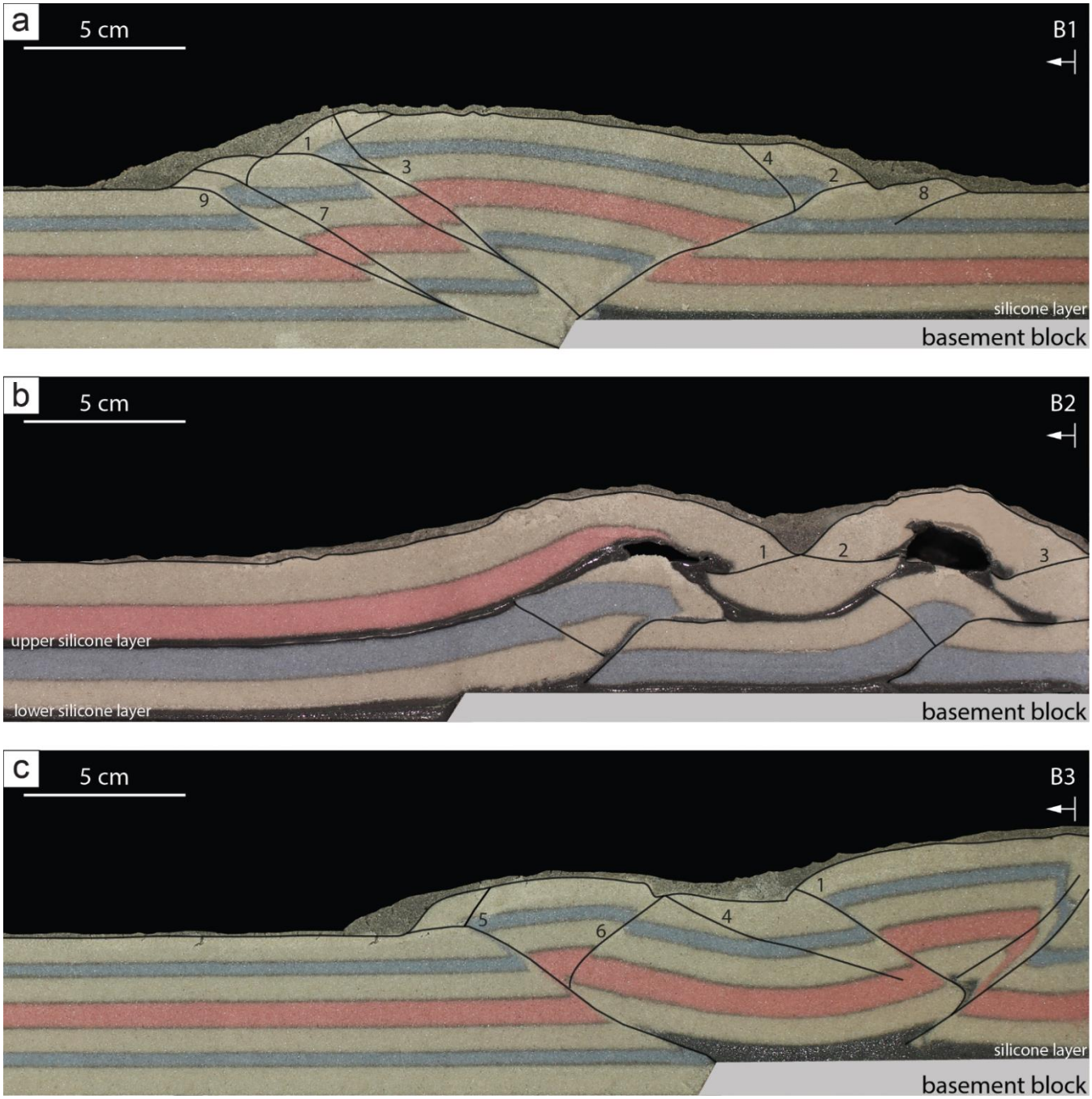

Figure 10: Side views of models (a) B1, (b) B2, and (c) B3 at 100 % of total shortening. Locations of sections are marked in Figure 9. Numbers show sequence of initial fault activityformation.

For model C, we used a basal plate geometry with three basal plates, aligned in an s-formincreased the number of basal plates to three, aligning them so that the margins of the plates formed one N-S and two E-W striking elements (Figure 7c). We placed silicone putty on both the basal plates and the table top, disconnecting it at the ramp to form a similar mechanical scenario as in model B3. Because of the larger size of the model, we increased the total shortening to 11 cm. Initially, a slightly asymmetrical pop-up structure formed close to the piston, with a back-thrust that migrated slightly upward along the main fore-thrust (2) (Figure 11a-b). Additional fore-thrusts (1, 3) developed especially in the northern area of the model, where the basal plate was missing. After ~ approximately 55% of total shortening, deformation propagated into the foreland, where a second asymmetrical pop-up structure formed above and parallel to the ramp in the subsurface. The master fore-thrust (5) accommodated most of the shortening,

whereas several minor back-thrusts migrated upward along the master thrust. The sand layer forms a ramp anticline over the master thrust, which approaches lower angles toward the surface. Close to reaching the total shortening, deformation propagated in the southern area of the model, where the basal plate reaches into the foreland, and third pop-up structure was formed there (9), but was not able to develop further with this amount of shortening. Overall, the wedge was relatively low compared to the brittle model A and the brittle-ductile model B1. The deformation front at total shortening approximately shows the contours of the basal plate in the centre and southern parts of the model (Figure 11a).

~~Calculation of mean shortening vectors via~~ PIV analysis of (surficial) shortening shows that ~~surface~~ deformation occurs in the tectonically active region west of the deformation front, with strain~~a~~ localisation ~~of strain~~ at the foremost thrust (2, 5, 9/10). ~~Vectors~~ Strain directions rotate outward on both the northern and southern side of the wedge. The dominant type of strain at the active fore-thrusts is shortening (red colours in Figure 11c). Extensional strain on top of the wedge (blue colours in Figure ~~10c~~11c) is mainly caused by gravitational collapse of parts of the wedge. We attribute local strike-slip strain (indicated by yellow to turquoise colors in Figure 11c) to erroneous vectors generated by the PIV analysis in areas where individual sand grains could not be tracked optically.~~More importantly, a~~A~~Along the entire deformation front, strike-slip strain (turquoise colours in Figure 11c) is subordinate to shortening, even in areas of the model where the trace of the deformation front is oblique to the direction of shortening.~~

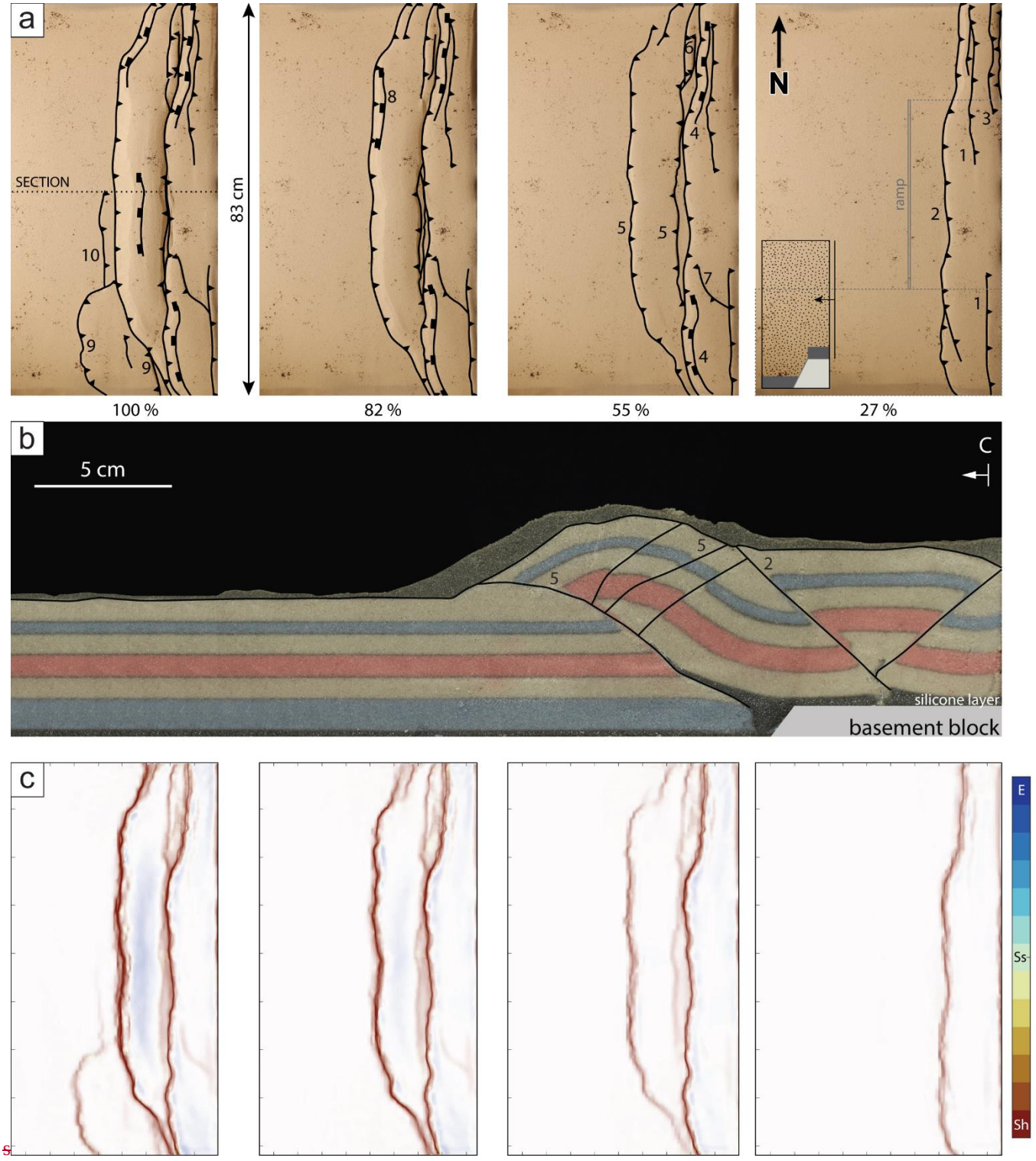

Figure 11: Modelling results of model C, showing (a) top views at 27, 55, 82 and 100 % of total shortening, and (b) side view at 100 % of total shortening. Numbers show sequence of ~~initial~~ fault ~~activity~~formation. (c) Analysis of cumulative strain showing s~~S~~train types ~~analysis~~ of model C~~, showing a~~. Areas of extension (E), strike-slip movement (Ss) and shortening (Sh). The inset in the first top view photograph shows the modelling setup in cross-sectional view.

For model D1 and D2 ~~the plate set-up was rotated, so that~~ shortening was directed at an angle of 45° to the basal plate and ramp (Figure 7c). Model C and D1 used an identical layering sequence ~~identical to model C~~. In the initial stages of the experiment (< ~~up to~~ 55% ~~of~~ total shortening), a pop-up structure developed over the entire length of the piston (Figure 12a). This structure~~In the~~

~~south of the model, the initial pop-up structure~~ is asymmetric with a main fore-thrust in the south.~~, whereas i~~ In the ~~centre~~ central area of the model, where the basal plate set-up creates a 90° angle, the structure is of a flip-type (see Smit et al., 2003, their Figure 4), where shortening was initially accommodated along a fore-thrust, before switching to a back-thrust. ~~The structures did not form entirely parallel to the piston, but f~~From approximately 27% of total shortening on, the wedge widened along the main fore-thrust (1) in the south, where the basal plate extends into the foreland, whereas in the centre and north of the model, shortening was accommodated by a series of ~~minor~~ fore-thrusts (3-5) that migrated along ~~their~~ an associated back-thrust. ~~The thrusts are more closely spaced within the corner between the plates.~~ From ~ 82% of total shortening~~With further shortening~~, the wedge propagated~~, first~~ on the southern basal plate (7) ~~from approximately 82% of total shortening~~, and ~~in a later stage~~ then on top of the northern plate (8). The surface expression of the propagating fore-thrusts runs parallel to the plate structure in the subsurface. ~~; whereas sections show that they~~The thrusts originate directly at the velocity discontinuity at the ramp (Figure 13a-b) and~~. The fore-thrusts~~ form ~~hinterland-dipping~~low-angle (~30°) master thrusts in strongly asymmetric pop-up structures, similar to model B3. ~~In contrast, in~~At the 90° corner between basal plates a steepening of the back thrust and migration of irregularly spaced fore-thrusts within the pop-up structure accommodate shortening ~~is completely accommodated within the initial pop-up structure with a steepening of the back thrust, caused by the confinement of the piston, and irregularly spaced fore thrusts that migrate, but do not propagate significantly~~. ~~In all cases, deformation does not propagate further than the velocity discontinuity and thus stays within the upper décollement level.~~

PIV analysis of ~~the~~ incremental displacements shows that shortening localises at the foremost thrust in model D1 (1, 7). ~~When analysing t~~The strain type patterns~~, the results~~ are similar to model C, with~~in the sense that~~ shortening ~~i~~as the dominant strain type ~~of strain~~, ~~independent of the orientation of the thrust trace, whereas the~~and the dominant strain direction ~~is mostly~~ perpendicular to the thrust trace. ~~As such, t~~The orientation of the basal plates in the subsurface evidently controls the orientation of the thrusts, with a local rotation~~g local~~ of the strain field~~, depending on the plate in the subsurface~~.

~~In m~~Model D2 used~~,~~ the same basal plate set-up ~~was used~~ as ~~in~~ model D1, ~~but we tested the effect of~~with a layering sequence using two ductile layers, similar to model B2 (Figure 7). Similar to model ~~D1~~B2, the upper and lower part of the model are decoupled ~~an initial pop-up structure formed at the wedge, featuring a main back-thrust within the lower part of the model, which is decoupled from the upper part~~ at the upper ductile layer. Propagation into the foreland occurred at~~swiftly, beginning ~~around~~~~ 55% of total shortening. In the lower part of the model, ~~resulting in~~ pop-up structures with a master fore-thrust ~~in the lower sand layer, which~~ localised at the ramp (Figures 12c, 13c). These ~~pop-up~~ structures form a sigmoidal shape that straddles the basal plate structure in the subsurface. ~~However, due to t~~The ~~strong~~ decoupling at the upper ductile layer caused that~~,~~ the surface structures ~~do not reflect the situation in the lower part of the model~~differ from the lower part of the model and the wedge reached far less height than in experiments with a single ductile layer.

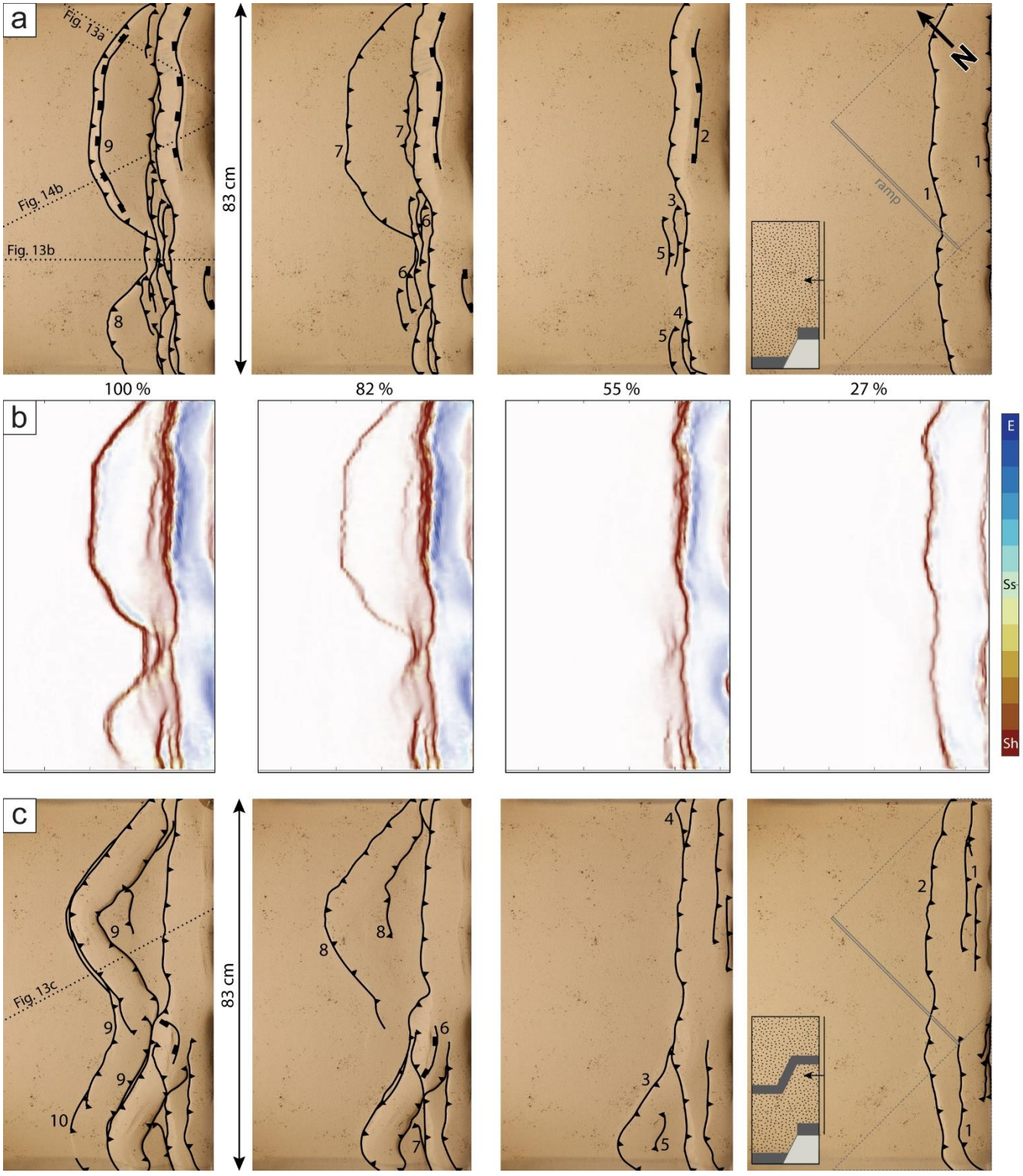

Figure 12: Top views of models (a) D1, and (c) D2 at 27, 55, 82 and 100 % of total shortening. Numbers show sequence of ~~initial~~ fault ~~activity~~formation. The insets in the first top view photographs show the modelling setups in cross-sectional view. PIV strain type analysis of model (b) D1, showing areas of extension (E), strike-slip movement (Ss) and shortening (Sh).

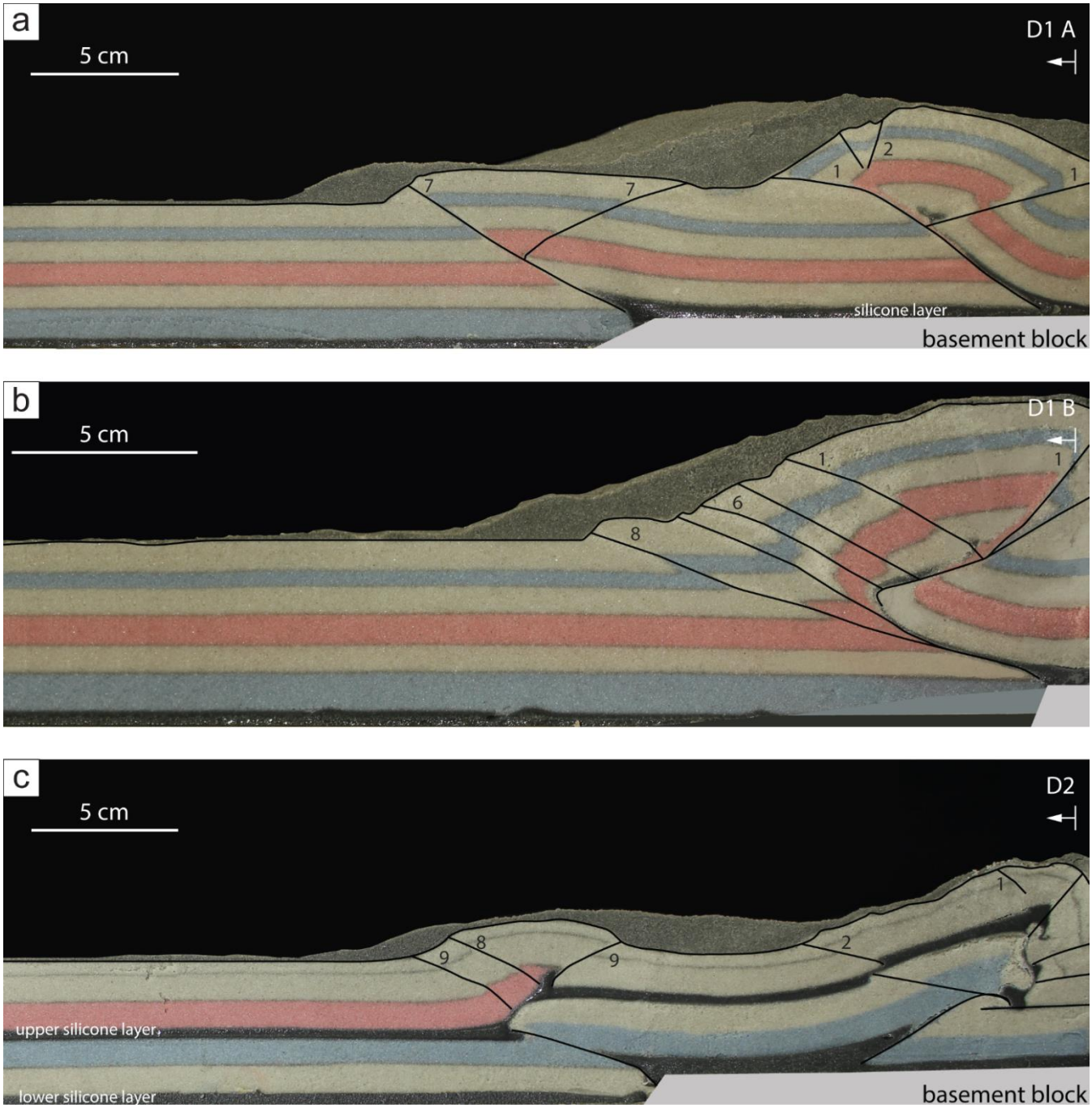

Figure 13: Side views of models (a, b) D1, and (c) D2 at 100 % of total shortening. Numbers show sequence of ~~initial~~ fault ~~activity~~formation.

5 Discussion

5.1 Analogue modelling

Inversion of basins, ~~either~~ whether orthogonal or oblique to the former basin margins, has been subject of many analogue modelling studies (e.g., Bonini et al., 2012; Brun & Nalpas, 1996; Del Ventisette et al., 2006; Deng et al., 2020; Molnar & Buiter, 2023; Sieberer et al., 2023; Yagupsky et al., 2008; Zwaan et al., 2022). The high variance of geological structures leads to a myriad of deformation styles characterizing inverted and reactivated fault systems (Bonini et al., 2012; their Figure 3), especially for inversional set-ups involving a viscous décollement (Brun & Nalpas, 1996). The modelling strategy (see Section 3.1) followed in

this study aimed to test ~~three~~ factors that may affect the structural grain of obliquely inverted extensional basins,~~. These factors~~ includinged the influence of 1) a weak basal décollement, and 2) pre-existing structures attributed to an extensional basin~~, and 3) thick-skinned or thin-skinned tectonics~~. The increasing complexity of the models is a result of consecutively implementing parameters that were found to be of relevance to the natural example, the Achental structure. Apart from its sigmoidal hanging wall shape, one of the complexities of the Achental structure is that its dominant fore-thrust is antithetic to the ~~existing~~ Jurassic normal fault in the subsurface (Figure 6). Most of the ~~deformational styles~~structures associated with basin inversion are synthetic to existing normal faults (e.g., Héja et al., 2022: their Figure 4 and 11; Bonini et al., 2012: their Figure 3), although the formation of an antithetic low-angle thrust has been ~~predicted~~ described (Laubscher, 1986; Tavarnelli, 1996) and ~~successfully~~ simulated in the context of thin-skinned deformation of the Jura fold and thrust belt (Caër et al., 2018).

5.1.1 Influence of mechanical stratigraphy

In our study, the influence of a weak basal décollement has been tested using two models (A~~1~~ and B1). These have an identical mechanical set-up, using a rigid ramp, which represents a pre-existing normal-fault controlled mechanical heterogeneity in the model and is pushed into a brittle (A~~1~~) or brittle-ductile (B1) cover. The ~~brittle model shows strong similarities to existing analogue experiments (e.g.,) and the~~ brittle-ductile model (B1)~~, but the latter~~ shows a narrower cross-sectional taper, a markedly lower angle of thrusting, wider thrust spacing and faster propagation compared to the brittle model (A). Decoupled thrust wedges are known to show these effects in nature (Jaumé & Lillie, 1988) and analogue models, attributed to a lower basal friction compared to frictional Coulomb wedges (Cotton & Koyi, 2000; Davis & Engelder, 1985; Mulugeta, 1988; Smit et al., 2003; Smit, 2005). ~~Comparing models A1 and B1~~Thus, ~~which were shortened orthogonally,~~ our brittle-ductile model B1 is able to better represent the low-angle character of the natural example than model A.

Models of oblique basin inversion show that the use of a ductile layer results in decoupling of the sedimentary cover and a strong localisation of deformation at existing extensional structures (e.g., Brun & Nalpas, 1996; Del Ventisette et al., 2006). Similarly, the use of an upper (second) ductile layer (models B2, D2) leads to a decoupling between the upper and lower sediment cover (e.g., Del Ventisette et al., 2006; Fan et al., 2020). As a result, structures within the lower brittle layer are terminated at the upper ductile layer~~, and do not reach the surface~~. ~~Consequently, l~~Low-angle hinterland-dipping thrusts emerging from the velocity discontinuity are therefore not visible in top view (see e.g., model D2, Figure 13). Decoupling thus prevents the formation of large-scale structures across the entire sedimentary cover.

5.1.2 Favourable kinematic conditions for basin inversion

The build-up of a certain height of the initial wedge at the backstop is a prerequisite for fault propagation, consistent with the critical taper theory of Davis et al. (1983) (see also Graveleau et al., 2012, and references therein). In all experiments, a wedge of 5.7–7.6 cm high was formed in front of the piston and at least 6 cm of shortening was needed for the thrusts to propagate into the foreland.

The movement of the basal plate (i.e., fixed or mobile, simulating thin- or thick-skinned deformation) then greatly influences the structure and location of the resulting wedge in brittle-ductile models (compare e.g., model B1 and B3). By using a mobile plate (model B1), this rigid block acts as a buttress, localis~~z~~ing early deformation at the ramp ~~already in the initial stages of the experiment, but also~~and restraining further movement of thrust sheets (Bailey et al., 2002; Gomes et al., 2010; Héja et al., 2022). ~~As a result, f~~Further shortening was accommodated along a main back-thrust with multiple fore-thrusts, showing strong similarities

to existing analogue experiments (e.g., Bonini et al., 2000; Persson & Sokoutis, 2002)., reflecting the relative movement of the sand layer opposite to the piston. The use of a fixed plate (model B3) represents a thin-skinned deformation style, where the sediment cover and basement are decoupled at a basal décollement. Deformation first localisesleads to initial strain localisation at the backstop (see also Caër et al., 2018; Deng et al., 2020; Yagupsky et al., 2008), but then propagates to the ramp. The mechanical contrast between the rigid ramp, quartz sand and silicone putty forms a velocity discontinuity (Allemand & Brun, 1991; Tron & Brun, 1991), which is crucial for secondary strain localisation during deformation. The step at the ramp, where silicone putty and quartz sand meet, thus works as a "fault generator" or a "nucleation site for thrust faulting" (Yagupsky et al., 2008, p. 852), not dissimilar to the "thrust mill" of Laubscher (1986), which is also demonstrated in models that use silicone putty or glass microbeads as a weak layer (Caër et al., 2018; Yagupsky et al., 2008). At the same time, structures localizsing at the ramp accommodate a large amount of shortening, preventing deformation from propagating further (Caër et al., 2018; Laubscher, 1986; Tavarnelli, 1996). Therefore, using a thin-skinned deformation style leads to the formation of aA low-angle fore-thrust that nucleates nucleating at the velocity discontinuity and thus may accommodates a great amount of shortening.

As a prerequisite for fault propagation, The initial wedge at the backstop needs to reach a certain height, analogue to the critical taper theory of. This theory is a popular approach to thrust system mechanics of (foreland) fold-and-thrust belts , and references therein). In all experiments, a wedge of 5.7–7.6 cm high was formed in front of the piston and at least 6 cm of shortening was needed for the thrusts to propagate into the foreland. An alternative approach was provided by, who used a sand prism at the back-stop as pre-existing hinterland topography for brittle-ductile models of basin inversion, resulting in an early propagation of deformation within 0.6 cm of shortening. The early evolution of our analogue models highlights the role of a fold-and-thrust belt in the hinterland for propagation of deformation.

5.1.3 Influence of structural inheritance

Although in all brittle-ductile models with a fixed plate an intial wedge formed parallel to the piston, pPropagation of deformation and strain localisation in brittle-ductile models led to the formation led to a series of structures that were oriented parallel to the basal plate boundaries in the subsurface. Other studiesModels of oblique shortening of pre-existing grabens or steps show similar results, where newly formed reverse and thrust faults more or less outline the structure in the subsurface (e.g., Caër et al., 2018; Deng et al., 2020; Molnar & Buiter, 2023; Yagupsky et al., 2008). Thrusts Whereas thrusts in models of Caër et al. (2018) appear to consistently dip towards the backstop.. However, Our PIV analyses of our models show that the dominant strain direction is approximately perpendicular to the thrust trace, which can be explained by strain partitioning mechanisms. The At the same time, the localisation of structures at steps and the geometry of the resulting low-angle fore-thrust with a hanging wall anticline (e.g., model D1, Figure 13a–b) is similar to the models of Caër et al. (2018; their Figure 4.11 b–e) and it is evident that in models with oblique shortening (model D1, D2) thrust faults outline the basal plate structure.

The obliquity angle between the basin axis and subsequent shortening has proven to greatly influences structures formed by basin inversion (Brun & Nalpas, 1996; Del Ventisette et al., 2006; Deng et al., 2020; Yagupsky et al., 2008). In purely brittle experiments, low obliquity angles are associated with an increasing angle of the reverse faults (Brun & Nalpas, 1996) and dominant fore-thrusts, whereas a higher obliquity angle preferably creates symmetrical pop-up structures (Deng et al., 2020). Our brittle-ductile models were able to create a dominant fore-thrust that localizes at the ramp regardless of the obliquity angle (90° for models B–C, 45° for models D). However, Ffault localisation at subsurface steps was most distinctive in models with a lower obliquity angle (45°, models D). Furthermore, oOur large-scale models (C and D) furthermore agree with those of Yagupsky et al. (2008) and Molnar and Buiter (2023), where the graben segment closest to the deformation front is reactivated first.

The analogue models (in particular models B3, C, D1; Figures 9c, 10b and 12a) ~~prove~~ show that low-angle hinterland-dipping thrusts can originate at~~from~~ a pre-existing high-angle normal fault with an opposite dip (see also Figure 6), as predicted (Laubscher, 1986; Tavarnelli, 1996). The~~A~~ pre-existing subsurface fault network ~~of extensional faults in the subsurface~~ is able to control the geometry of inversion structures ~~related to its inversion~~. ~~Furthermore, t~~The models exemplify that through strain localisation ~~of the thrusts~~ at ~~the~~ subsurface steps~~ramps in the subsurface~~, the sigmoidal geometry of the Achental thrust hanging wall (see model series D, Figure 12) can be created within a single deformation phase ~~and with a single direction~~ of oblique shortening.

5.2 Comparison with the natural example

In analogue models we aim to create a scaled and simplified version of the natural example, the Achental structure. ~~In the models w~~We show that it is possible to form a sigmoidal structure, characterized by a low-angle main fore-thrust, hanging wall anticlines and a localisation at a pre-existing step, within a single phase of shortening (Figure 14). Model parameters that were found to be applicable to the Achental structure are 1) ~~the presence of~~ a weak basal décollement, 2) thin-skinned deformation, and 3) a clear velocity discontinuity ~~at the frontal ramp~~ acting as a "fault generator". However, laboratory experiments cannot fully encompass the complexities of natural geological structures. In this section, we compare features of the analogue models and the Achental structure.

5.2.1 Mechanical stratigraphy

Rheological ~~properties~~ heterogeneity of ~~the~~ sedimentary successions are important parameters for both analogue models and natural processes. A brittle-ductile succession is able to re-create large-scale structures in analogue models. However, small-scale faulting and folding within the sedimentary cover of the NCA is ~~"lost in translation"~~cannot be reproduced by the analogue models (see also Figure 14b). Comparison between brittle and brittle-ductile models shows that a very weak décollement is imperative for the low-angle Achental thrust to form at a pre-existing basement step. Whether or not this décollement is present in the hanging wall of the original normal fault, does not influence strain localisation ~~of deformation~~ in the models, although it might impact fault propagation with further shortening (Caër et al., 2018). An offset of the décollement, as opposed to a monocline across the ramp (model B2), increases the effect of the velocity discontinuity, but is not strictly necessary for localisation to occur. The Haselgebirge-Reichenhall succession at the base of the Karwendel thrust sheet ~~consisting mostly of rock salt~~ forms the main décollement of the NCA (Eisbacher & Brandner, 1995)~~, providing the required weak basal layer~~. ~~The Kössen~~An intermediate succession of Carnian shales, evaporites and carbonates (Raibl Fm) may also be represented by a ductile layer, decoupling the lower and upper carbonate platform. Kilian et al. (2021) argue that in this part of the NCA, the Carnian units mostly consist of carbonates (e.g., Brandner & Poleschinski, 1986; Jerz, 1966), which we modelled as competent units. ~~However,~~Our analogue models with two detachment horizons show a complete decoupling between the upper and lower brittle section~~that structures in the lower section do not connect to the upper section~~. Although in the Achental structure, small-scale folding dies out near the Hauptdolomit-Plattenkalk transition, the overall geometry of the Unnutz anticline is preserved through the entire outcropping sedimentary succession. Therefore, we dismiss the hypothesis that the Raibl Fm behaves as a significant decoupling horizon~~ductile material~~.

~~Because c~~Carbonate units ~~of~~ within the Achental structure are represented by quartz sand in analogue models, simulating brittle behaviour. This modelling material is not able~~, the models are not able~~ to simulate folding of the Guffert-Unnutz-Montscheinspitze anticline. Resulting from the chosen modelling materials and scaling, important features of the natural example, e.g., the large

overturned panels seen in the cross-sections (Figures 5 and 14), cannot be explained by the analogue models. However, the thinning of strata in the hanging wall, close to the fault, could be reproduced (Figure 14b). Ortner (2003a) proposes a progressive rollover-fault-propagation model (Storti & Salvini, 1996) for the Unnutz anticline. This type of folding leads to strongly overturned or recumbent anticlines in fold-and-thrust belts (Storti & Salvini, 1996) and involves a fault-propagation fold with strong, layer-parallel shear (flexural slip). Although for fault-propagation folds "important field evidence […] is the observation that some faults, particularly thrust faults, die out in the cores of folds." (Suppe, 1985, p. 350), this is not necessarily the case for progressive rollover-fault-propagation folds, because the overturned limb of the hanging wall anticline has been completely detached from the footwall (Storti & Salvini, 1996: Fig. 2). Flexural slip accommodating deformation within the Guffert-Unnutz-Montscheinspitze anticline is seen from layer-parallel and very low-angle fault planes within Hauptdolomit, and support the progressive rollover-fault-propagation model. Fault-propagation folding as a mechanism is seen in the La Roche d'Or anticline, Swiss Alps (Caër et al., 2018), which. This anticline formed along a thrust fault that, in depth, localises originating at a basement step attributed to extensional faulting, thus showing strong similarities to the Achental structure. Similar to the Reichenhall-Haselgebirge succession in the NCA, evaporitic sediments form a décollement between the basement and the sediment cover. Martin and Mercier (1996) provide a natural example of the western Jura, showing the development of a low-angle ramp above pre-existing structures of the Bresse graben. While the progressive rollover-fault-propagation model produces overturned panels, it does not explain e.g., the hinge collapse interpreted for the Unnutz anticline (Figure 5a). Although thinning of the overturned limb is expected and can be seen in the analogue models as well (Figure 14b), the complete elimination of stratigraphy in the overturned flank of the anticline cannot be explained by this type of folding.

In salt-detached fold-and-thrust belts the structural style is among others dependent on the amount of salt available (Hudec & Jackson, 2007; Lacombe et al., 2019). Within salt-controlled belts, anticlines are mostly (faulted) detachment folds, which can be mistaken as fault-propagation folds due to their superficial resemblance (Mitra, 2002). Detachment folding (e.g., Epard & Groshong, 1995; Homza & Wallace, 1995; Josep Poblet, 1996) and subsequent truncation and displacement of these folds (e.g., Jamison, 1987; Morley, 1994; Suppe & Medwedeff, 1990) produces asymmetric anticlines with steep to overturned forelimbs (Wallace & Homza, 2004). In the case of salt-related structures (e.g., minibasins), shortening will initially concentrate on these structures (Duffy et al., 2018; Snidero et al., 2019). Reactivation of salt welds as thrusts and rotation of flaps may produce overturned panels with incomplete stratigraphy (Duffy et al., 2018; Granado et al., 2019; Granado et al., 2021; Rowan & Vendeville, 2006). The exact type of deformation strongly depends on the original thickness of the Haselgebirge-Reichenhall succession. In the case of the Achental structure is it unknown how much salt was present originally. If a substantial amount was available, it might have controlled the geometry of overlying younger deposits. However, no major growth wedges or angular unconformities have been observed in the area up to now.

5.2.2 Kinematic parameters and structural inheritance

In analogue models, the use of a fixed basal plate translates to a thin-skinned tectonic style, in which the sedimentary cover is decoupled from the basement by a décollement (Rodgers, 1949). Such thin-skinned structural style is well known from the NCA (e.g., Auer & Eisbacher, 2003; Eisbacher et al., 1990). However, fFor a correct localisation and propagation of deformation, the presence of a step in the subsurface and topography in the hinterland is important as well. Keeping in mind model scaling, Early Cretaceous topography must have existed at no more than ~ 14 km SE of the Jurassic normal fault. The advancing front of the NCA fold-and-thrust belt and the uplift resulting from movement along e.g., the NW verging Eben thrust (Eisbacher & Brandner, 1996) (Figure 1b) may have provided this topography. Within the subsurface, tThe Jurassic basin architecture in the subsurface is thought to have provided steps where deformation could localise (Figure 14a). Thickness and fFacies differentiations of Jurassic

sediments, a maximum thickness of Upper Jurassic sediments in the overstep area between the Karwendel and Thiersee synclines (Figure 1c) (Nagel et al., 1976; K.-I. Schütz, 1979), and documented Cretaceous transport directions oblique to the synclines (Ortner & Gruber, 2011; Sausgruber, 1994a, 1994b) underline the presence of such a basin (see Section 2.2). We assume that, corresponding to~~Following~~ the geometry of the Achental structure, at least one N–S striking, west-dipping normal fault ~~must have been oriented approximately N-S.~~and two E–W trending s~~S~~trike-slip faults ~~trending~~ must have existed~~E-W~~ (Eisbacher & Brandner, 1995, 1996) ~~may form additional steps~~ (Figure 14a). Such a basin geometry is similar to Jurassic fault systems in more western parts of the Alpine orogen (Eberli, 1985, 1987; Weissert & Bernoulli, 1985) and has been proposed for the Achensee region (Channell et al., 1990; Eisbacher & Brandner, 1995, 1996).

The models were subjected to a single phase of oblique shortening, simulating NW-directed Cretaceous convergence related to Alpine orogeny. Field data from the Achensee area (Beer, 2003; Sausgruber, 1994b) support ~~the influence of~~ NW-directed shortening. ~~On the other hand,~~ Ortner and Gruber (2011) argue that the offset in the central Achental thrust is larger than in its northern and southern thrust segments, and ~~that~~ therefore the direction of shortening must have been < 270°. Because the orientation of the folds (e.g., the Thiersee syncline; Töchterle, 2005) and faults within the Achental structure is oblique to Cretaceous shortening (e.g., Eisbacher & Brandner, 1996), many studies have offered alternative hypotheses involving multiple deformation phases and directions (e.g., Ampferer, 1921; Auer, 2001; Channell et al., 1990; Channell et al., 1992; Fuchs, 1944; Ortner, 2003a; Spengler, 1953). Although t~~T~~he formation of the Guffert-Unnutz-Montscheinspitze anticline and the Achental thrust is ascribed to pre-Gosau, deformation (Ortner & Gruber, 2011; Töchterle, 2005), ~~which~~ this is no proof~~does not prove~~ that the entire sigmoidal hanging wall formed during a NW direction of shortening. However, in our models we re-create the geometry of the Achental structure (including a low-angle thrust antithetic to the assumed subsurface step, and a a surface expression of the hanging wall outlining the subsurface geometry) by applying shortening at 45° to the N–S trending Jurassic fault, demonstrating that a single uniform phase of oblique shortening is sufficient to create a sigmoidal shape of the hanging wall that outlines the subsurface basin geometry of the Achental structure, as depicted in Figure 14. Our results thus agree with the hypothesis that the characteristic shape of the Achental structure formed due to forced folding at the borders of a Jurassic basin (Eisbacher & Brandner, 1995, 1996; Ortner & Gruber, 2011).

5.3 Limitations

The NCA are a salt-influenced fold-and-thrust belt with at least one (basal) décollement consisting of a pre-rift evaporitic succession. We chose to model this décollement ~~include~~ as a relatively thin layer of iron powder-dosed silicone putty at the base of a thick, brittle sedimentary cover. However, geological settings often do not show ideal ("layer-cake") stratigraphic geometries. In salt-influenced regions, diapirs may create e.g., minibasins or flaps (e.g., Rowan et al., 2016). Using non-layer-cake geometries in physical experiments produces structures that are much different from classical thin-skinned fold-and-thrust belts (e.g., Rowan & Vendeville, 2006) and thus the classical layer-cake approach may lead to misinterpretation (Lacombe et al., 2019). In the central and eastern NCA the role of salt tectonics has been addressed by an increasing number of (recent) studies (e.g., Fernández et al., 2021; Fernández et al., 2022; Granado et al., 2019; Granado et al., 2021; Santolaria et al., 2022; Strauss et al., 2021). Resulting structural styles are highly complex and include km-scale overturned panels and missing stratigraphy (Granado et al., 2019). The amount of salt available in salt-influenced fold-and-thrust belts controls the type of structures that can form during inversion (Hudec & Jackson, 2007; Lacombe et al., 2019). Triassic growth strata caused by salt tectonics have been reported for the central and eastern NCA, and locally in the western NCA (Fernández et al., 2021; Fernández et al., 2022; Granado et al., 2019; Granado et al., 2021; Kilian et al., 2021; Kilian & Ortner, 2019; Ortner & Kilian, 2022; Santolaria et al., 2022; Strauss et al., 2021), but there are no reliable estimates on the thickness of the Haselgebirge-Reichenhall succession underneath the Achental structure. The main

goal of our modelling approach was to gain insight in conditions controlling strain localization and associated folding and thrusting at pre-existing basin boundaries in an oblique convergent setting. We did not aim to include the complexity of salt tectonics in our models, therefore a silicone putty has been mixed that does not favour diapir formation. Introducing Triassic salt dynamics to our models would then create e.g., flaps and minibasins. Hypothetically, if the overturned panels originally were flaps onlapping salt diapirs, localisation of folding and thrusting would have been easier, as diapirs would localize thrusts. In such a case, the Jurassic basin geometry would have an even more profound effect on structures at the original basin margins.

~~One~~ Another limitation of the analogue models compared to the natural example is that we did not consider Paleogene reactivation of Cretaceous structures. Paleogene folding however, is common throughout the Achental structure and Achensee area. E.g., the Hofjoch, Blaubergalm and Seekar folds (Figure 4) (Brandner & Gruber, 2011; Eisbacher & Brandner, 1995; Sausgruber, 1994b) show an orientation corresponding to post-Cretaceous shortening. The Seekar folds are offset by the N–S striking Seekar fault, which shows dextral strike-slip movement and a P-axis that corresponds to NNE- to NE-directed Paleogene shortening. Paleogene reactivation of fault planes also occurs at the west side of the Achensee (Sausgruber, 1994b). Although this post-Cretaceous reactivation may have imprinted on existing structures, we propose that the rough outlines of the Achental structure were established after Cretaceous orogeny (Figure 14a).

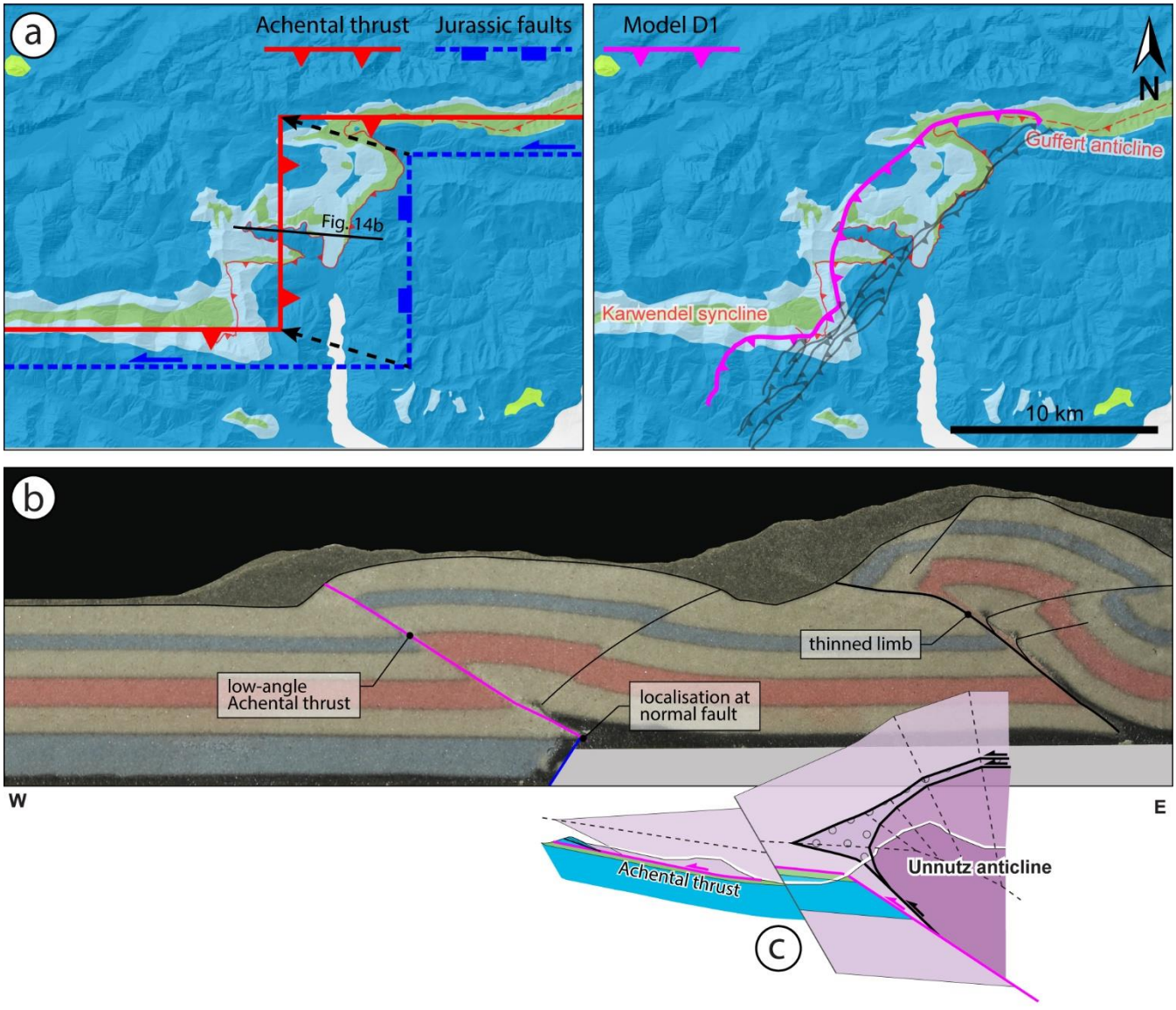

Figure 14: Summary figure showing (a) possible arrangement of Jurassic basin-bounding faults in relation to the Achental thrust (left) and overlay of inversion structures formed in analogue model D1, outlining the subsurface architecture (right). The trace of the thrust in model D1 has not been intersected with the topography. Geological map ~~M~~modified after Ortner and Gruber (2011) and Ortner and Kilian (2016). For legend of background figure, see Figure 1. (b) shows key structural elements in a cross-section of model D1 and (c) the corresponding cross-section of the Unnutz anticline (see also Figure 5a). The Achental thrust is marked in pink. See Figure 5 for legend of lithologies.

6 Conclusions

Analogue models were used to infer favourable kinematic and mechanic conditions for the oblique inversion of a pre-existing extensional basin margin. Yet relevant for understanding deformation geometries arising from oblique basin inversion in general, the modelling results have been discussed in the frame of the Achental structure in the European Alps, which evolved from the inversion of the Jurassic Achental basin during ~~Alpine~~ Cretaceous and Paleogene orogenic phases~~y~~. The modelling set-up wa~~s~~ based on the assumption that the Achental basin in the subsurface of the Achental structure consists of at least (1) an approximately N–S trending, W-dipping normal fault, and (2) two E–W trending additional strike-slip faults. Furthermore, we applied~~y~~ a thin-skinned style of deformation and shortening at 45° to the Jurassic structures, which both characterise Cretaceous orogeny in the NCA. ~~Based on the modelling results we conclude~~

The modelling results show that the basal ductile décollement of the NCA ~~:~~

~~1) A thin-skinned style of deformation that characterises Cretaceous orogeny in the NCA and leads to the formation of a fold-and-thrust belt in the hinterland, provides the structural framework for propagation of deformation to the basin margins,~~

~~2) The Jurassic basin geometry consists of When applying shortening at 45° to the Jurassic structures, newly formed thrusts then form along these steps.~~

~~3) The sedimentary cover is represented by a brittle succession that is separated from the basement by ductile décollement, the~~ (Haselgebirge-Reichenhall succession), which separated the basement from a predominantly brittle cover, ~~. This basal décollement~~ is crucial for the decoupling of the sedimentary cover. ~~and~~ The ~~is together with the~~ mechanical contrast across the basin bounding normal fault then control~~l~~~~sing~~ ~~the~~ deformation localisation ~~of a low-angle thrust dipping opposite to the inherited normal fault, the Achental thrust~~at the existing fault step. As a result,

~~When these parameters are applied, a~~a low-angle thrust (Achental thrust), antithetic to the Jurassic normal fault, ~~is formed due to thrust localisation~~forms at the eastern margin of the Achental basin. The hanging wall geometry of this thrust~~, the Achentaler Schubmasse,~~ outlines the ~~Jurassic~~ basin architecture in the subsurface, ~~proving~~ exemplifying ~~that~~ the control of the pre-existing ~~extensional fault~~structural framework~~s~~ on ~~are a controlling factor for~~ structures that form during subsequent ~~–~~shortening. We therefore show that ~~Thus,~~ a single phase of Cretaceous oblique shortening at 45° to the Jurassic Achental basin axis is sufficient to form a sigmoidal geometry of the hanging wall (Achentaler Schubmasse). In a broader framework, we conclude that when shortening is applied oblique to existing basin boundaries, strain localisation leads to the formation of new thrusts along the steps formed by these structures.

Author contributions

The conceptualization of the study was done by HO and EW; Field investigations were performed by WvK, HO, AG and TS; Analogue modelling was planned and performed by WvK, EW and DS; Data preparation, analysis and visualisation were performed by WvK; WvK prepared the original draft of the manuscript with input from all co-authors; All co-authors reviewed and edited the manuscript and approved the final version.

Competing interests

At least one of the (co-)authors is a guest member of the editorial board of Solid Earth and has collaborated as a (co-)author on publications involving one of the guest editors of Solid Earth. The peer-review process was guided by an independent editor, and the authors have also no other competing interests to declare.

Acknowledgements

This work was completed as part of a Master Thesis at the University of Innsbruck. The University of Innsbruck through a needs-based scholarship provided financial support covering fieldwork and travel expenses. Laboratory experiments were conducted at the TecLab of Utrecht University. Klaus Pelz and an anonymous reviewer have provided valuable feedback, which has considerably improved the quality of this work. We sincerely thank Antoine Auzemery for assistance with the conceptualization and realization of analogue experiments, and Taco Broerse for his help with the Strainmap package, as well as fruitful discussions. We also thank Lukas Schifferle for assistance during fieldwork and digitalization. The authors thank Midland Valley for providing their Move Software in the frame of their academic software initiative and the state of Tyrol for providing high resolution hilllshades.

References

Allemand, P., & Brun, J.-P. (1991). Width of continental rifts and rheological layering of the lithosphere. *Tectonophysics*, *188*(1-2), 63–69. https://doi.org/10.1016/0040-1951(91)90314-I

Allen, J., & Beaumont, C. (2016). Continental margin syn-rift salt tectonics at intermediate width margins. *Basin Research*, *28*(5), 598–633. https://doi.org/10.1111/bre.12123

Amilibia, A., McClay, K. R., Sàbat, F., Muñoz, J. A., & Roca, E. (2005). Analogue modelling of inverted oblique rift systems. *Geologica Acta*, 251. https://doi.org/10.1344/105.000001395

Ampferer, O. (1902). Über den geologischen Zusammenhang des Karwendel- und Sonnwendgebirges. *Verhandlungen Der Kaiserlich-Königlichen Geologischen Reichsanstalt*, 104–113.

Ampferer, O. (1921). Über NW-Beanspruchungen in den Nordalpen. *Jahrbuch Der Geologischen Bundesanstalt*, *71*, 198–202.

Ampferer, O. (1941). Tektonische Nachbarschaft Karwendel-Sonnwendgebirge. *Sitzungsberichte Der Akademie Der Wissenschaften in Wien, Mathematisch-Naturwissenschaftliche Klasse*, *150*, 181–199.

Ampferer, O., & Heissel, G. (1950). *Geologische Karte des östlichen Karwendel und des Achensee-Gebietes*. Innsbruck: Universitätsverlag Wagner.

Auer, M. (2001). Struktur und Kinematik der nördlichen Kalkalpen im TRANSALP-Profil (Südbayern, Nordtirol) (Dissertation). Universität Karlsruhe, Karlsruhe.

Auer, M., & Eisbacher, G. H. (2003). Deep structure and kinematics of the Northern Calcareous Alps (TRANSALP Profile). *Geologische Rundschau*, *92*(2), 210–227. https://doi.org/10.1007/s00531-003-0316-0

Bailey, C. M., Giorgis, S., & Coiner, L. (2002). Tectonic inversion and basement buttressing: an example from the central Appalachian Blue Ridge province. *Journal of Structural Geology*, *24*(5), 925–936. https://doi.org/10.1016/S0191-8141(01)00102-X

Bechstädt, T., & Mostler, H. (1974). Mikrofazies und Mikrofauna mitteltriadischer Beckensedimente der Nördlichen Kalkalpen Tirols. *Geologisch-Paläontologische Mitteilungen Universität Innsbruck*, *4*(5/6), 1–74.

Beer, E. (2003). Vergleichende tektonische Untersuchungen an zwei längsalpinen Störungen: der Achentaler Schubmasse und der Salzachstörung (Doctoral thesis). Ludwig-Maximilians-Universität München, Munich, Germany.

Bernoulli, D., & Jenkyns, H. C. (1974). Alpine, Mediterranean, and Central Atlantic Mesozoic facies in relation to the early evolution of the Tethys. In R. H. Dott & R. H. Shaver (Eds.), *Modern and Ancient Geosynclinal Sedimentation* (pp. 129–160). SEPM (Society for Sedimentary Geology). https://doi.org/10.2110/pec.74.19.0129

Bonini, M. (1998). Chronology of deformation and analogue modelling of the Plio-Pleistocene 'Tiber Basin': implications for the evolution of the Northern Apennines (Italy). *Tectonophysics*, *285*(1-2), 147–165. https://doi.org/10.1016/S0040-1951(97)00189-3

Bonini, M., Sani, F., & Antonielli, B. (2012). Basin inversion and contractional reactivation of inherited normal faults: A review based on previous and new experimental models. *Tectonophysics*, *522-523*, 55–88. https://doi.org/10.1016/j.tecto.2011.11.014

Bonini, M., Sokoutis, D., Mulugeta, G., & Katrivanos, E. (2000). Modelling hanging wall accommodation above rigid thrust ramps. *Journal of Structural Geology*, *22*(8), 1165–1179. https://doi.org/10.1016/S0191-8141(00)00033-X

Brandner, R., & Gruber, A. (2011). Exkursion E2a - Rofangebirge. In A. Gruber (Ed.), *Arbeitstagung 2011 "Geologie des Achenseegebietes". Geologisches Kartenblatt 88* (pp. 149–167). Wien: Geologische Bundesanstalt.

Brandner, R., Lotter, M., Gruber, A., & Ortner, H. (2011). Exkursion E3 – Achental – Bächental. Donnerstag, 22.09.2011. In A. Gruber (Ed.), *Arbeitstagung 2011 "Geologie des Achenseegebietes". Geologisches Kartenblatt 88* (pp. 199–224). Wien: Geologische Bundesanstalt.

Brandner, R., & Poleschinski, W. (1986). Stratigraphie und Tektonik am Kalkalpensüdrand zwischen Zirl und Seefeld in Tirol (Exkursion D am 3. April 1986). *Jahresberichte Und Mitteilungen Des Oberrheinischen Geologischen Vereins*, *68*, 67–92. https://doi.org/10.1127/jmogv/68/1986/67

Broerse, T. (2021). Strainmap.

Broerse, T., Krstekanić, N., Kasbergen, C., & Willingshofer, E. (2021). Mapping and classifying large deformation from digital imagery: application to analogue models of lithosphere deformation. *Geophysical Journal International*, *226*(2), 984–1017. https://doi.org/10.1093/gji/ggab120

Brun, J.-P. (1999). Narrow rifts versus wide rifts: inferences for the mechanics of rifting from laboratory experiments. *Philosophical Transactions of the Royal Society of London. Series a: Mathematical, Physical and Engineering Sciences*, *357*(1753), 695–712. https://doi.org/10.1098/rsta.1999.0349

Brun, J.-P., & Nalpas, T. (1996). Graben inversion in nature and experiments. *Tectonics*, *15*(3), 677–687. https://doi.org/10.1029/95TC03853

Buchanan, P. G., & McClay, K. R. (1992). Experiments on basin inversion above reactivated domino faults. *Marine and Petroleum Geology*, *9*(5), 486–500. https://doi.org/10.1016/0264-8172(92)90061-I

Buiter, S. J. H., & Pfiffner, A. O. (2003). Numerical models of the inversion of half-graben basins. *Tectonics*, *22*(5), 1057. https://doi.org/10.1029/2002TC001417

Caër, T., Souloumiac, P., Maillot, B., Leturmy, P., & Nussbaum, C. (2018). Propagation of a fold-and-thrust belt over a basement graben. *Journal of Structural Geology*, *115*, 121–131. https://doi.org/10.1016/j.jsg.2018.07.007

Channell, J., Brandner, R., & Spieler, A. (1990). Mesozoic paleogeography of the Northern Calcareous Alps—Evidence from paleomagnetism and facies analysis. *Geology*, *18*(9), 828. https://doi.org/10.1130/0091-7613(1990)018<0828:MPOTNC>2.3.CO;2

Channell, J., Brandner, R., Spieler, A., & Stoner, J. S. (1992). Paleomagnetism and paleogeography of the Northern Calcareous Alps (Austria). *Tectonics*, *11*(4), 792–810. https://doi.org/10.1029/91TC03089

Cooper, M., & Warren, M. J. (2020). Inverted fault systems and inversion tectonic settings. In N. Scarselli, J. Adam, D. Chiarella, D. G. Roberts, & A. W. Bally (Eds.), *Regional Geology and Tectonics: Principles of Geologic Analysis* (pp. 169–204). Elsevier. https://doi.org/10.1016/B978-0-444-64134-2.00009-2

Cotton, J. T., & Koyi, H. A. (2000). Modeling of thrust fronts above ductile and frictional detachments: Application to structures in the Salt Range and Potwar Plateau, Pakistan. *Geological Society of America Bulletin*, *112*(3), 351–363. https://doi.org/10.1130/0016-7606(2000)112<351:MOTFAD>2.0.CO;2

Davis, D. M., & Engelder, T. (1985). The role of salt in fold-and-thrust belts. *Tectonophysics*, *119*(1-4), 67–88. https://doi.org/10.1016/0040-1951(85)90033-2

Davis, D. M., Suppe, J., & Dahlen, F. A. (1983). Mechanics of fold-and-thrust belts and accretionary wedges. *Journal of Geophysical Research: Solid Earth*, *88*(B2), 1153. https://doi.org/10.1029/JB088iB02p01153

Del Ventisette, C., Montanari, D., Sani, F., & Bonini, M. (2006). Basin inversion and fault reactivation in laboratory experiments. *Journal of Structural Geology*, *28*(11), 2067–2083. https://doi.org/10.1016/J.JSG.2006.07.012

Del Ventisette, C., Montanari, D., Sani, F., Bonini, M., & Corti, G. (2007). Reply to comment by J. Wickham on "Basin inversion and fault reactivation in laboratory experiments". *Journal of Structural Geology*, *29*(8), 1417–1418. https://doi.org/10.1016/j.jsg.2007.05.003

Deng, H., Koyi, H. A., & Zhang, J. (2020). Modelling oblique inversion of pre-existing grabens. *Geological Society, London, Special Publications*, *487*(1), 263–290. https://doi.org/10.1144/SP487.5

Dombrádi, E., Sokoutis, D., Bada, G., Cloetingh, S., & Horváth, F. (2010). Modelling recent deformation of the Pannonian lithosphere: Lithospheric folding and tectonic topography. *Tectonophysics*, *484*(1-4), 103–118. https://doi.org/10.1016/j.tecto.2009.09.014

Donofrio, D. A., Brandner, R., & Poleschinski, W. (2003). Conodonten der Seefeld-Formation: ein Beitrag zur Bio- und Lithostratigraphie der Hauptdolomit-Plattform (Obertrias, westliche Nördliche Kalkalpen, Tirol. *Geologisch-Paläontologische Mitteilungen Universität Innsbruck*, *26*, 91–107.

Dubois, A., Odonne, F., Massonnat, G., Lebourg, T., & Fabre, R. (2002). Analogue modelling of fault reactivation: tectonic inversion and oblique remobilisation of grabens. *Journal of Structural Geology*, *24*(11), 1741–1752. https://doi.org/10.1016/S0191-8141(01)00129-8

Duffy, O. B., Dooley, T. P., Hudec, M. R., Jackson, M. P., Fernandez, N., Jackson, C. A.-L., & Soto, J. I. (2018). Structural evolution of salt-influenced fold-and-thrust belts: A synthesis and new insights from basins containing isolated salt diapirs. *Journal of Structural Geology*, *114*, 206–221. https://doi.org/10.1016/j.jsg.2018.06.024

Eberli, G. P. (1985). Die jurassischen Sedimente in den ostalpinen Decken Graubündens: Relikte eines passiven Kontinentalrandes (Thesis). ETH Zurich.

Eberli, G. P. (1987). Carbonate turbidite sequences deposited in rift-basins of the Jurassic Tethys Ocean (eastern Alps, Switzerland). *Sedimentology*, *34*(3), 363–388. https://doi.org/10.1111/j.1365-3091.1987.tb00576.x

Eberli, G. P., Bernoulli, D., Sanders, D., & Vecsei, A. (1993). From aggradation to progradation: The Maiella platform, Abruzzi, Italy. In T. Simo & R. W. Scott (Eds.), *AAPG Memoir: Vol. 56. Cretaceous Carbonate Platforms.*

Eisbacher, G. H., & Brandner, R. (1995). Role of high-angle faults during heteroaxial contraction, Inntal thrust sheet, Northern Calcareous Alps, western Austria. *Geologisch-Paläontologische Mitteilungen Universität Innsbruck*, *20*, 389–406.

Eisbacher, G. H., & Brandner, R. (1996). Superposed fold-thrust structures and high-angle faults, Northwestern Calcareous Alps, Austria. *Eclogae Geologicae Helvetiae*, *89*, 553–571.

Eisbacher, G. H., Linzer, H.-G., & Meier, L. (1990). A depth extrapolated structural transect across the Northern Calcareous Alps of Western Tirol. *Eclogae Geologicae Helvetiae*, *83*(3), 711–725.

Epard, J.-L., & Groshong, R. H. (1995). Kinematic model of detachment folding including limb rotation, fixed hinges and layer-parallel strain. *Tectonophysics*, *247*(1-4), 85–103. https://doi.org/10.1016/0040-1951(94)00266-C

Etheridge, M. A. (1986). On the reactivation of extensional fault systems. *Philosophical Transactions of the Royal Society of London. Series A, Mathematical and Physical Sciences*, *317*(1539), 179–194. https://doi.org/10.1098/rsta.1986.0031

Fan, X., Jia, D., Yin, H., Shen, L., Liu, J., & Cui, J., et al. (2020). Analogue modeling of the northern Longmen Shan thrust belt (eastern margin of the Tibetan plateau) and strain analysis based on Particle Image Velocimetry. *Journal of Asian Earth Sciences*, *198*, 104238. https://doi.org/10.1016/j.jseaes.2020.104238

Faupl, P., & Wagreich, M. (1999). Late Jurassic to Eocene Palaeogeography and Geodynamic Evolution of the Eastern Alps. *Mitteilungen Der Österreichischen Geologischen Gesellschaft*, *92*, 79–94.

Fernández, O., Grasemann, B., & Sanders, D. (2022). Deformation of the Dachstein Limestone in the Dachstein thrust sheet (Eastern Alps, Austria). *Austrian Journal of Earth Sciences*, *115*(1), 167–190. https://doi.org/10.17738/ajes.2022.0008

Fernández, O., Habermüller, M., & Grasemann, B. (2021). Hooked on salt: Rethinking Alpine tectonics in Hallstatt (Eastern Alps, Austria). *Geology*, *49*(3), 325–329. https://doi.org/10.1130/g47981.1

Froitzheim, N., & Manatschal, G. (1996). Kinematics of Jurassic rifting, mantle exhumation, and passive-margin formation in the Austroalpine and Penninic nappes (eastern Switzerland). *Geological Society of America Bulletin*, *108*(9), 1120–1133. https://doi.org/10.1130/0016-7606(1996)108<1120:KOJRME>2.3.CO;2

Froitzheim, N., Schmid, S. M., & Conti, P. (1994). Repeated change from crustal shortening to orogen-parallel extension in the Austroalpine units of Graubünden. Advance online publication. https://doi.org/10.5169/seals-167471

Fruth, I., & Scherreiks, R. (1982). Hauptdolomit (Norian) — stratigraphy, paleogeography and diagenesis. *Sedimentary Geology*, *32*(3), 195–231. https://doi.org/10.1016/0037-0738(82)90050-1

Fuchs, A. (1944). Untersuchungen am tektonischen Gefüge der Tiroler Alpen. II. (Kalkalpen Achensee – Kaisergebirge). *Neues Jahrb. Für Mineral. Etc. Abh., Abt. B*, *88*, 337–373.

Gawlick, H.-J. (2004). Definition of the Tauglboden Formation (Oxfordian to Tithonian) in the Tauglboden Basin (Northern Calcareous Alps). *Berichte Des Institutes Für Erdwissenschaften Der Karl-Franzens-Universität Graz*, *9*(127-129).

Giles, K. A., & Rowan, M. G. (2012). Concepts in halokinetic-sequence deformation and stratigraphy. *Geological Society, London, Special Publications*, *363*(1), 7–31. https://doi.org/10.1144/SP363.2

Golebiowski, R. (1991). *Becken und Riffe der alpinen Obertrias. Lithostratigraphie und Biofazies der Kössener Formation: Exkursionen im Jungpaläozoikum und Mesozoikum Österreichs*. Wien: Österreichische Paläontologische Gesellschaft.

Gomes, C. J., Danderfer Filho, A., Posada, A. M. A., & Da Silva, A. C. (2010). The role of backstop shape during inversion tectonics physical models. *Anais Da Academia Brasileira De Ciências*, *82*(4), 997–1012. https://doi.org/10.1590/S0001-37652010000400021

Granado, P., Roca, E., Strauss, P., Pelz, K., & Muñoz, J. A. (2019). Structural styles in fold-and-thrust belts involving early salt structures: The Northern Calcareous Alps (Austria). *Geology*, *47*(1), 51–54. https://doi.org/10.1130/G45281.1

Granado, P., Ruh, J. B., Santolaria, P., Strauss, P., & Muñoz, J. A. (2021). Stretching and Contraction of Extensional Basins With Pre-Rift Salt: A Numerical Modeling Approach. *Frontiers in Earth Science*, *9*. https://doi.org/10.3389/feart.2021.648937

Graveleau, F., Malavieille, J., & Dominguez, S. (2012). Experimental modelling of orogenic wedges: A review. *Tectonophysics*, *538-540*, 1–66. https://doi.org/10.1016/j.tecto.2012.01.027

Gruber, A. (2011). *Geological manuscript map ÖK 88 Achenkirch: Unveröff. Manuskriptkarte*. Wien: Geologische Bundesanstalt.

Gruber, A., Lotter, M., & Geologische Bundesanstalt. (2022). *Erläuterungen zu Blatt 88 Achenkirch*. *Geologische Karte der Republik Österreich [Geologische Karte Österreich / Erläuterungen] : Erläuterungen*. Wien: Geologische Bundesanstalt.

Gümbel, C. W. (1861). *Geognostische Beschreibung des bayerischen Alpengebirges und seines Vorlandes*. Gotha: Perthes.

Haas, J., Kovács, S., Krystyn, L., & Lein, R. (1995). Significance of Late Permian-Triassic facies zones in terrane reconstructions in the Alpine-North Pannonian domain. *Tectonophysics*, *242*(1-2), 19–40. https://doi.org/10.1016/0040-1951(94)00157-5

Héja, G., Ortner, H., Fodor, L., Németh, A., & Kövér, S. (2022). Modes of Oblique Inversion: A Case Study from the Cretaceous Fold and Thrust Belt of the Western Transdanubian Range (TR), West Hungary. *Tectonics*, *41*(3). https://doi.org/10.1029/2021TC006728

Homza, T. X., & Wallace, W. K. (1995). Geometric and kinematic models for detachment folds with fixed and variable detachment depths. *Journal of Structural Geology*, *17*(4), 575–588. https://doi.org/10.1016/0191-8141(94)00077-D

Hubbert, M. K. (1937). Theory of scale models as applied to the study of geologic structures. *Geological Society of America Bulletin*, *48*(10), 1459–1520. https://doi.org/10.1130/GSAB-48-1459

Hudec, M. R., & Jackson, M. P. (2007). Terra infirma: Understanding salt tectonics. *Earth-Science Reviews*, *82*(1-2), 1–28. https://doi.org/10.1016/j.earscirev.2007.01.001

Jamison, W. R. (1987). Geometric analysis of fold development in overthrust terranes. *Journal of Structural Geology*, *9*(2), 207–219. https://doi.org/10.1016/0191-8141(87)90026-5

Jaumé, S. C., & Lillie, R. J. (1988). Mechanics of the Salt Range-Potwar Plateau, Pakistan: A fold-and-thrust belt underlain by evaporites. *Tectonics*, *7*(1), 57–71. https://doi.org/10.1029/TC007i001p00057

Jerz, H. (1966). Untersuchungen über Stoffbestand, Bildungsbedingungen und Paläogeographie der Raibler Schichten zwischen Lech und Inn (Nördl. Kalkalpen). *Geologica Bavarica*, *56*, 3–100.

Josep Poblet, K. M. (1996). Geometry and Kinematics of Single-Layer Detachment Folds. *AAPG Bulletin*, *80*. https://doi.org/10.1306/64ED8CA0-1724-11D7-8645000102C1865D

Kilian, S. (2013). Bericht 2012 über geologische und strukturgeologische Aufnahmen im Karwendelgebirge auf Blatt 2223 Innsbruck und auf Blatt 2217 Hinterriß. *Jahrbuch Der Geologischen Bundesanstalt*, *153*, 411–417.

Kilian, S., & Ortner, H. (2019). Structural evidence of in-sequence and out-of-sequence thrusting in the Karwendel mountains and the tectonic subdivision of the western Northern Calcareous Alps. *Austrian Journal of Earth Sciences*, *112*(1), 62–83. https://doi.org/10.17738/ajes.2019.0005

Kilian, S., Ortner, H., & Schneider-Muntau, B. (2021). Buckle folding in the Northern Calcareous Alps - Field observations and numeric experiments. *Journal of Structural Geology*, *150*, 104416. https://doi.org/10.1016/j.jsg.2021.104416

Kley, J., Rossello, E. A., Monaldi, C. R., & Habighorst, B. (2005). Seismic and field evidence for selective inversion of Cretaceous normal faults, Salta rift, northwest Argentina. *Tectonophysics*, *399*(1-4), 155–172. https://doi.org/10.1016/J.TECTO.2004.12.020

Konstantinovskaya, E. A., Harris, L. B., Poulin, J., & Ivanov, G. M. (2007). Transfer zones and fault reactivation in inverted rift basins: Insights from physical modelling. *Tectonophysics*, *441*(1-4), 1–26. https://doi.org/10.1016/j.tecto.2007.06.002

Koopman, A., Speksnijder, A., & Horsfield, W. T. (1987). Sandbox model studies of inversion tectonics. *Tectonophysics*, *137*(1-4), 379–388. https://doi.org/10.1016/0040-1951(87)90329-5

Krainer, K., Lucas, S. G., & Strasser, M. (2011). Vertebrate Fossils from the Northalpine Raibl Beds, Western Northern Calcareous Alps, Tyrol (Austria). *Austrian Journal of Earth Sciences*, *104*(1), 97–106.

Krstekanić, N., Willingshofer, E., Broerse, T., Matenco, L., Toljić, M., & Stojadinovic, U. (2021). Analogue modelling of strain partitioning along a curved strike-slip fault system during backarc-convex orocline formation: Implications for the Cerna-Timok fault system of the Carpatho-Balkanides. *Journal of Structural Geology*, *149*, 104386. https://doi.org/10.1016/j.jsg.2021.104386

Krstekanić, N., Willingshofer, E., Matenco, L., Toljić, M., & Stojadinovic, U. (2022). The influence of back-arc extension direction on the strain partitioning associated with continental indentation: Analogue modelling and implications for the Circum-Moesian Fault System of South-Eastern Europe. *Journal of Structural Geology*, *159*, 104599. https://doi.org/10.1016/j.jsg.2022.104599

Lackschewitz, K. S., Grützmacher, U., & Henrich, R. (1991). Paleoceanography and rotational block faulting in the Jurassic carbonate series of the Chiemgau Alps (Bavaria). *Facies*, *24*(1), 1–23. https://doi.org/10.1007/BF02536838

Lacombe, O., Mazzoli, S., Hagke, C. von, Rosenau, M., Fillon, C., & Granado, P. (2019). Style of deformation and tectono-sedimentary evolution of fold-and-thrust belts and foreland basins: From nature to models. *Tectonophysics*, *767*, 228163. https://doi.org/10.1016/j.tecto.2019.228163

Laubscher, H. P. (1986). The eastern Jura: Relations between thin-skinned and basement tectonics, local and regional. *Geologische Rundschau*, *75*(3), 535–553. https://doi.org/10.1007/BF01820630

Lee, A. R., & Warren, J. B. (1940). A coni-cylindrical viscometer for measuring the visco-elastic characteristics of highly viscous liquids. *Journal of Scientific Instruments*, *17*(3), 63–67. https://doi.org/10.1088/0950-7671/17/3/303

Leever, K. A., Gabrielsen, R. H., Faleide, J. I., & Braathen, A. (2011). A transpressional origin for the West Spitsbergen fold-and-thrust belt: Insight from analog modeling. *Tectonics*, *30*(2), n/a-n/a. https://doi.org/10.1029/2010TC002753

Lein, R. (1987). Evolution of the Northern Calcareous Alps during Triassic times. In H. W. Flügel & P. Faupl (Eds.), *Geodynamics of the Eastern Alps* (pp. 85–102). Wien: Deuticke.

Leitner, C., & Neubauer, F. (2011). Tectonic significance of structures within the salt deposits Altaussee and Berchtesgaden–Bad Dürrnberg, Northern Calcareous Alps. *Austrian Journal of Earth Sciences*, *104*(2), 2–21.

Lemoine, M., Bas, T., Arnaud-Vanneau, A., Arnaud, H., Dumont, T., & Gidon, M., et al. (1986). The continental margin of the Mesozoic Tethys in the Western Alps. *Marine and Petroleum Geology*, *3*(3), 179–199. https://doi.org/10.1016/0264-8172(86)90044-9

Lipold, M. W. (1854). Der Salzberg am Dürrnberg nächst Hallein. *Jahrbuch Der Kaiserlich-Königlichen Geologischen Reichsanstalt*, *5*, 590–610.

Manger, G. E. (1963). *Porosity and bulk density of sedimentary rocks.* (Geological Survey Bulletin No. 1144-E).

Martin, J., & Mercier, E. (1996). Heritage distensif et structuration chevauchante dans une chaine de couverture; apport de l'equilibrage par modelisation geometrique dans le Jura nord-occidental. *Bulletin De La Société Géologique De France*, *167*(1), 101–110.

Merle, O., & Abidi, N. (1995). Approche experimentale du fonctionnement des rampes emergentes. *Bulletin De La Société Géologique De France*, *166*(5), 439–450. https://doi.org/10.2113/gssgfbull.166.5.439

Mitra, S. (2002). Structural models of faulted detachment folds. *AAPG Bulletin*, *86*. https://doi.org/10.1306/61EEDD3C-173E-11D7-8645000102C1865D

Mojsisovics, E. von. (1871). Beiträge zur topischen Geologie der Alpen. *Jahrbuch Der Geologischen Reichsanstalt*, *21*, 189–210.

Molnar, N., & Buiter, S. (2023). Analogue modelling of the inversion of multiple extensional basins in foreland fold-and-thrust belts. *Solid Earth*, *14*(2), 213–235. https://doi.org/10.5194/se-14-213-2023

Mooney, M., & Ewart, R. H. (1934). The Conicylindrical Viscometer. *Physics*, *5*(11), 350–354. https://doi.org/10.1063/1.1745219

Morley, C. K. (1994). Fold-generated imbricates: examples from the Caledonides of Southern Norway. *Journal of Structural Geology*, *16*(5), 619–631. https://doi.org/10.1016/0191-8141(94)90114-7

Müller-Jungbluth, W.-U. (1968). Sedimentary Petrologic Investigation of the Upper Triassic "Hauptdolomit" of the Lechtaler Alps, Tyrol, Austria. In G. Müller & G. M. Friedman (Eds.), *Recent Developments in Carbonate Sedimentology in Central Europe* (pp. 228–239). Berlin, Heidelberg: Springer Berlin Heidelberg.

Mulugeta, G. (1988). Modelling the geometry of Coulomb thrust wedges. *Journal of Structural Geology*, *10*(8), 847–859. https://doi.org/10.1016/0191-8141(88)90099-5

Nagel, K.-H. (1975). *Der Bau der Thiersee- und Karwendelmulde (Tirol)*. *Geotektonische Forschungen: Vol. 48*. Stuttgart.

Nagel, K.-H., Schütz, K.-I., Schütz, S., Wilmers, W., & Zeil, W. (1976). Die geodynamische Entwicklung der Thiersee- und der Karwendelmulde (Nördliche Kalkalpen). *Geologische Rundschau*, *65*, 536–557.

Nielsen, S. B., & Hansen, D. L. (2000). Physical explanation of the formation and evolution of inversion zones and marginal troughs. *Geology*, *28*(10), 875. https://doi.org/10.1130/0091-7613(2000)28<875:PEOTFA>2.0.CO;2

Ortner, H. (2001). Growing folds and sedimentation of the Gosau Group, Muttekopf, Northern Calcareous Alps, Austria. *Geologische Rundschau*, *90*(3), 727–739. https://doi.org/10.1007/s005310000182

Ortner, H. (2003a). Cretaceous thrusting in the western part of the Northern Calcareous Alps (Austria) - evidences from synorogenic sedimentation and structural data. *Mitteilungen Der Österreichischen Geologischen Gesellschaft*, *94*(2001), 63–77.

Ortner, H. (2003b). Local and far field stress-analysis of brittle deformation in the western part of the Northern Calcareous Alps, Austria. *Geologisch-Paläontologische Mitteilungen Universität Innsbruck*, *26*, 109–136.

Ortner, H. (2016). Field trip 4 Deep water sedimentation on top of a growing orogenic wedge - interaction of thrusting, erosion and deposition in the Cretaceous Northern Calcareous Alps. *Geo.Alp*, *13*, 141–182.

Ortner, H., & Gaupp, R. (2007). Synorogenic sediments of the western Northern Calcareous Alps. *Geo.Alp*, *4*, 133–148.

Ortner, H., & Gruber, A. (2011). 3D-Geometrie der Strukturen zwischen Karwendel-Synklinale und Thiersee-Synklinale. In A. Gruber (Ed.), *Arbeitstagung 2011 "Geologie des Achenseegebietes". Geologisches Kartenblatt 88* (pp. 51–67). Wien: Geologische Bundesanstalt.

Ortner, H., & Kilian, S. (2016). Sediment creep on slopes in pelagic limestones: Upper Jurassic of Northern Calcareous Alps, Austria. *Sedimentary Geology*, *344*, 350–363. https://doi.org/10.1016/J.SEDGEO.2016.03.013

Ortner, H., & Kilian, S. (2022). Thrust tectonics in the Wetterstein and Mieming mountains, and a new tectonic subdivision of the Northern Calcareous Alps of Western Austria and Southern Germany. *Geologische Rundschau*, *111*(2), 543–571. https://doi.org/10.1007/s00531-021-02128-3

Ortner, H., Kositz, A., Willingshofer, E., & Sokoutis, D. (2016). Geometry of growth strata in a transpressive fold belt in field and analogue model: Gosau Group at Muttekopf, Northern Calcareous Alps, Austria. *Basin Research*, *28*(6), 731–751. https://doi.org/10.1111/bre.12129

Ortner, H., & Sieberer, A.-K. (2022). From foreland thrust belt to accretionary wedge: Synorogenic sediments monitor a changing geodynamic setting in the Northern Calcareous Alps of the European Eastern Alps. *EGU General Assembly 2022, Vienna, Austria, 23–27 May 2022*, EGU22-11281. https://doi.org/10.5194/egusphere-egu22-11281

Ortner, H., Ustaszewski, M., & Rittner, M. (2008). Late Jurassic tectonics and sedimentation: breccias in the Unken syncline, central Northern Calcareous Alps. *Swiss Journal of Geosciences*, *101*(S1), 55–71. https://doi.org/10.1007/s00015-008-1282-0

Persson, K. S., & Sokoutis, D. (2002). Analogue models of orogenic wedges controlled by erosion. *Tectonophysics*, *356*(4), 323–336. https://doi.org/10.1016/S0040-1951(02)00443-2

Quenstedt, W. (1933). Studien in der Überschiebungszone von Achenkirch. *Zeitschrift Der Deutschen Geologischen Gesellschaft*, *85*, 459–461.

Ramberg, H. (1981). *Gravity, deformation and the earth's crust: In theory, experiments and geological application* (2nd ed.). London: Academic Press.

Riedel, P. (1988). Facies and development of the ‘wilde kirche’ reef complex (Rhaetian, Upper Triassic, Karwendelgebirge, Austria). *Facies*, *18*(1), 205–217. https://doi.org/10.1007/BF02536800

Rodgers, J. (1949). Evolution of Thought on Structure of Middle and Southern Appalachians. *AAPG Bulletin*, *33*. https://doi.org/10.1306/3D933E00-16B1-11D7-8645000102C1865D

Rowan, M. G., Giles, K. A., Hearon IV, T. E., & Fiduk, J. C. (2016). Megaflaps adjacent to salt diapirs. *AAPG Bulletin*, *100*(11), 1723–1747. https://doi.org/10.1306/05241616009

Rowan, M. G., & Vendeville, B. C. (2006). Foldbelts with early salt withdrawal and diapirism: Physical model and examples from the northern Gulf of Mexico and the Flinders Ranges, Australia. *Marine and Petroleum Geology*, *23*(9-10), 871–891. https://doi.org/10.1016/j.marpetgeo.2006.08.003

Rüffer, T., & Zühlke, R. (1995). Sequence Stratigraphy and Sea-Level Changes in the Early to Middle Triassic of the Alps: A Global Comparison. In B. Haq (Ed.), *Sequence Stratigraphy and Depositional Response to Eustatic, Tectonic and Climatic Forcing* (pp. 161–207). Dordrecht: Kluwer.

Santolaria, P., Granado, P., Wilson, E. P., Matteis, M. de, Ferrer, O., & Strauss, P., et al. (2022). From Salt-Bearing Rifted Margins to Fold-And-Thrust Belts. Insights from Analog Modeling and Northern Calcareous Alps Case Study. *Tectonics*, *41*(11). https://doi.org/10.1029/2022TC007503

Sassi, W., Colletta, B., Balé, P., & Paquereau, T. (1993). Modelling of structural complexity in sedimentary basins: The role of pre-existing faults in thrust tectonics. *Tectonophysics*, *226*(1-4), 97–112. https://doi.org/10.1016/0040-1951(93)90113-X

Sausgruber, T. (1994a). Bericht 1993 über geologische Aufnahmen in den Nördlichen Kalkalpen auf Blatt 88 Achenkirch. *Jahrbuch Der Geologischen Bundesanstalt*, *137*, 469.

Sausgruber, T. (1994b). Jurabeckenentwicklung nördlich vom Achensee und deren Folgen bei der alpidischen Kompressionstektonik (Diploma thesis). Leopold-Franzens Universität Innsbruck, Innsbruck.

Schmid, S. M., Bernoulli, D., Fügenschuh, B., Matenco, L., Schefer, S., & Schuster, R., et al. (2008). The Alpine-Carpathian-Dinaridic orogenic system: correlation and evolution of tectonic units. *Swiss Journal of Geosciences*, *101*(1), 139–183. https://doi.org/10.1007/s00015-008-1247-3

Schmid, S. M., Fügenschuh, B., Kissling, E., & Schuster, R. (2004). Tectonic map and overall architecture of the Alpine orogen. *Eclogae Geologicae Helvetiae*, *97*(1), 93–117. https://doi.org/10.1007/s00015-004-1113-x

Schmid, S. M., Pfiffner, A. O., Froitzheim, N., Schönborn, G., & Kissling, E. (1996). Geophysical-geological transect and tectonic evolution of the Swiss-Italian Alps. *Tectonics*, *15*(5), 1036–1064. https://doi.org/10.1029/96TC00433

Schuster, R., Daurer, A., Krenmayr, H. G., Linner, M., Mandl, G. W., Pestal, G., & Reitner, J. M. (2019). *Rocky Austria: The Geology of Austria - brief and colourful* (3. Auflage, revidierte Ausgabe). Wien: GeoSphere Austria.

Schütz, K.-I. (1979). Die Aptychenschichten der Thiersee- und der Karwendel-Mulde. *Geotektonische Forschungen*, *57*, 1–84.

Sibson, R. H. (1995). Selective fault reactivation during basin inversion: potential for fluid redistribution through fault-valve action. *Geological Society, London, Special Publications*, *88*(1), 3–19. https://doi.org/10.1144/GSL.SP.1995.088.01.02

Sieberer, A.-K., Willingshofer, E., Klotz, T., Ortner, H., & Pomella, H. (2023). Inversion of extensional basins parallel and oblique to their boundaries: inferences from analogue models and field observations from the Dolomites Indenter, European eastern Southern Alps. *Solid Earth*, *14*(7), 647–681. https://doi.org/10.5194/se-14-647-2023

Smit, J. H. W. (2005). Brittle-ductile coupling in thrust wedges and continental transforms (Doctoral thesis). VU Amsterdam & Université de Rennes, Amsterdam, Rennes.

Smit, J. H. W., Brun, J.-P., & Sokoutis, D. (2003). Deformation of brittle-ductile thrust wedges in experiments and nature. *Journal of Geophysical Research: Solid Earth*, *108*(B10). https://doi.org/10.1029/2002JB002190

Snidero, M., Muñoz, J. A., Carrera, N., Butillé, M., Mencos, J., & Motamedi, H., et al. (2019). Temporal evolution of the Darmadan salt diapir, eastern Fars region, Iran. *Tectonophysics*, *766*, 115–130. https://doi.org/10.1016/j.tecto.2019.06.006

Sokoutis, D., Bonini, M., Medvedev, S., Boccaletti, M., Talbot, C. J., & Koyi, H. A. (2000). Indentation of a continent with a built-in thickness change: experiment and nature. *Tectonophysics*, *320*(3-4), 243–270. https://doi.org/10.1016/S0040-1951(00)00043-3

Sokoutis, D., Burg, J.-P., Bonini, M., Corti, G., & Cloetingh, S. (2005). Lithospheric-scale structures from the perspective of analogue continental collision. *Tectonophysics*, *406*(1-2), 1–15. https://doi.org/10.1016/J.TECTO.2005.05.025

Spengler, E. (1953). Versuch einer Rekonstruktion des Ablagerungsraumes der nördlichen Kalkalpen (1. Teil, Westabschnitt). *Jahrbuch Der Geologischen Bundesanstalt*, *96*, 1–64.

Spengler, E. (1956). Versuch einer Rekonstruktion des Ablagerungsraumes der nördlichen Kalkalpen (2. Teil, Mittelabschnitt). *Jahrbuch Der Geologischen Bundesanstalt*, *99*, 1–74.

Spieler, A. (1994). Bericht 1993 über geologische Aufnahmen in den Nördlichen Kalkalpen auf Blatt 88 Achenkirch. *Jahrbuch Der Geologischen Bundesanstalt*, *137*, 474–475.

Spieler, A. (1995). *Geological manuscript map.*

Spieler, A., & Brandner, R. (1989). Vom Jurassischen Pull-apart Becken zur Westüberschiebung der Achentaler Schubmasse (Tirol, Österreich). *Geologisch-Paläontologische Mitteilungen Universität Innsbruck*, *16*, 191–194.

Spötl, C. (1989). The Alpine Haselgebirge Formation, Northern Calcareous Alps (Austria): Permo-Scythian evaporites in an alpine thrust system. *Sedimentary Geology*, *65*(1-2), 113–125. https://doi.org/10.1016/0037-0738(89)90009-2

Stampfli, G., Mosar, J., Marquer, D., Marchant, R., Baudin, T., & Borel, G. (1998). Subduction and obduction processes in the Swiss Alps. *Tectonophysics*, *296*(1-2), 159–204. https://doi.org/10.1016/S0040-1951(98)00142-5

Storti, F., & Salvini, F. (1996). Progressive Rollover Fault-Propagation Folding: A Possible Kinematic Mechanism to Generate Regional-Scale Recumbent Folds in Shallow Foreland Belts. *AAPG Bulletin*, *80*. https://doi.org/10.1306/64ED8782-1724-11D7-8645000102C1865D

Strauss, P., Granado, P., & Muñoz, J. A. (2021). Subsidence analysis of salt tectonics-driven carbonate minibasins (Northern Calcareous Alps, Austria). *Basin Research*, *33*(2), 968–990. https://doi.org/10.1111/bre.12500

Stüwe, K., & Schuster, R. (2010). Initiation of subduction in the Alps: Continent or ocean? *Geology*, *38*(2), 175–178. https://doi.org/10.1130/G30528.1

Suppe, J. (1985). *Principles of structural geology*. Englewood Cliffs, New Jersey: Prentice-Hall.

Suppe, J., & Medwedeff, D. A. (1990). Geometry and kinematics of fault-propagation folding. *Eclogae Geologicae Helvetiae*, *83*, 409–454. Retrieved from https://api.semanticscholar.org/CorpusID:131023185

Tavarnelli, E. (1996). The effects of pre-existing normal faults on thrust ramp development: An example from the northern Apennines, Italy. *Geologische Rundschau*, *85*(2), 363–371. https://doi.org/10.1007/BF02422241

Thielicke, W. (2014). The Flapping Flight of Birds - Analysis and Application (PhD thesis). Rijksuniversiteit Groningen, Groningen, Netherlands. Retrieved from http://irs.ub.rug.nl/ppn/382783069

Thielicke, W., & Sonntag, R. (2021). Particle Image Velocimetry for MATLAB: Accuracy and enhanced algorithms in PIVlab. *Journal of Open Research Software*, *9*(1), 12. https://doi.org/10.5334/jors.334

Thielicke, W., & Stamhuis, E. J. (2014). PIVlab – Towards User-friendly, Affordable and Accurate Digital Particle Image Velocimetry in MATLAB. *Journal of Open Research Software*, *2*. https://doi.org/10.5334/jors.bl

Thorwart, M., Dannowski, A., Grevemeyer, I., Lange, D., Kopp, H., & Petersen, F., et al. (2021). Basin inversion: reactivated rift structures in the central Ligurian Sea revealed using ocean bottom seismometers. *Solid Earth*, *12*(11), 2553–2571. https://doi.org/10.5194/se-12-2553-2021

Töchterle, A. (2005). Tektonische Entwicklungsgeschichte des Südteiles der Nördlichen Kalkalpen entlang der TRANSALP-Tiefenseismik anhand bilanzierter Profile (Diploma thesis). Leopold-Franzens Universität Innsbruck, Innsbruck.

Tong, H., & an Yin. (2011). Reactivation tendency analysis: A theory for predicting the temporal evolution of preexisting weakness under uniform stress state. *Tectonophysics*, *503*(3-4), 195–200. https://doi.org/10.1016/j.tecto.2011.02.012

Tron, V., & Brun, J.-P. (1991). Experiments on oblique rifting in brittle-ductile systems. *Tectonophysics*, *188*(1-2), 71–84. https://doi.org/10.1016/0040-1951(91)90315-J

Turner, J. P., & Williams, G. A. (2004). Sedimentary basin inversion and intra-plate shortening. *Earth-Science Reviews*, *65*, 277–304.

Ulrich, R. (1960). Die Entwicklung der ostalpinen Juraformation im Vorkarwendel zwischen Mittenwald und Achensee. *Geologica Bavarica*, *41*, 99–151.

Van Gelder, I. E., Willingshofer, E., Sokoutis, D., & Cloetingh, S. (2017). The interplay between subduction and lateral extrusion: A case study for the European Eastern Alps based on analogue models. *Earth and Planetary Science Letters*, *472*, 82–94. https://doi.org/10.1016/j.epsl.2017.05.012

Wallace, W. K., & Homza, T. X. (2004). Detachment folds versus fault-propagation folds, and their truncation by thrust faults. In K. R. McClay (Ed.), *AAPG Memoir: Vol. 82. Thrust tectonics and hydrocarbon systems* (pp. 324–355).

Weijermars, R. (1986a). Finite strain of laminar flows can be visualized in SGM36-polymer. *Naturwissenschaften*, *73*(1), 33–34. https://doi.org/10.1007/BF01168803

Weijermars, R. (1986b). Flow behaviour and physical chemistry of bouncing putties and related polymers in view of tectonic laboratory applications. *Tectonophysics*, *124*(3-4), 325–358. https://doi.org/10.1016/0040-1951(86)90208-8

Weijermars, R. (1986c). Polydimethylsiloxane flow defined for experiments in fluid dynamics. *Applied Physics Letters*, *48*(2), 109–111. https://doi.org/10.1063/1.97008

Weijermars, R., Jackson, M., & Vendeville, B. C. (1993). Rheological and tectonic modeling of salt provinces. *Tectonophysics*, *217*(1-2), 143–174. https://doi.org/10.1016/0040-1951(93)90208-2

Weijermars, R., & Schmeling, H. (1986). Scaling of Newtonian and non-Newtonian fluid dynamics without inertia for quantitative modelling of rock flow due to gravity (including the concept of rheological similarity). *Physics of the Earth and Planetary Interiors*, *43*(4), 316–330. https://doi.org/10.1016/0031-9201(86)90021-X

Weissert, H. J., & Bernoulli, D. (1985). A transform margin in the Mesozoic Tethys: evidence from the Swiss Alps. *Geologische Rundschau*, *74*(3), 665–679. https://doi.org/10.1007/BF01821220

Wickham, J. (2007). Comment on "Basin inversion and fault reactivation in laboratory experiments". *Journal of Structural Geology*, *29*(8), 1414–1416. https://doi.org/10.1016/j.jsg.2007.05.002

Willingshofer, E., Neubauer, F., & Cloetingh, S. (1999). The significance of Gosau-type basins for the late cretaceous tectonic history of the Alpine-Carpathian belt. *Physics and Chemistry of the Earth, Part a: Solid Earth and Geodesy*, *24*(8), 687–695. https://doi.org/10.1016/S1464-1895(99)00100-3

Willingshofer, E., Sokoutis, D., Beekman, F., Schönebeck, J.-M., Warsitzka, M., & Rosenau, M. (2018). *Ring shear test data of feldspar sand and quartz sand used in the Tectonic Laboratory (TecLab) at Utrecht University for experimental Earth Science applications.*

Willingshofer, E., Sokoutis, D., & Burg, J.-P. (2005). Lithospheric-scale analogue modelling of collision zones with a pre-existing weak zone. *Geological Society, London, Special Publications*, *243*(1), 277–294. https://doi.org/10.1144/gsl.sp.2005.243.01.18

Yagupsky, D. L., Cristallini, E. O., Fantín, J., Valcarce, G. Z., Bottesi, G., & Varadé, R. (2008). Oblique half-graben inversion of the Mesozoic Neuquén Rift in the Malargüe Fold and Thrust Belt, Mendoza, Argentina: New insights from analogue models. *Journal of Structural Geology*, *30*(7), 839–853. https://doi.org/10.1016/j.jsg.2008.03.007

Zorlu, J. (2007). Sedimentpetrographische und geochemische Untersuchungen an unterschiedlich überprägten Triasdolomiten der Ost- und Südalpen (Doctoral thesis). Ruhr-Universität Bochum, Bochum.

Zwaan, F., Schreurs, G., Buiter, S. J. H., Ferrer, O., Reitano, R., Rudolf, M., & Willingshofer, E. (2022). Analogue modelling of basin inversion: a review and future perspectives. *Solid Earth*, *13*(12), 1859–1905. https://doi.org/10.5194/se-13-1859-2022